Ideal Triangle Groups, Dented Tori, and Numerical Analysis

Richard Evan Schwartz *

May 18, 2003

Abstract

We prove the Goldman-Parker Conjecture: A complex hyperbolic ideal triangle group is discretely embedded in $PU(2,1)$ if and only if the product of its three standard generators is not elliptic. We also prove that such a group is indiscrete if the product of its three standard generators is elliptic. A novel feature of this paper is that it uses a rigorous computer assisted proof to deal with difficult geometric estimates.

1 Introduction

A basic problem in geometry and representation theory is the *deformation problem*. Suppose that $\rho_0 : \Gamma \to G_1$ is a discrete embedding of a finitely generated group Γ into a Lie group G_1. Suppose also that $G_1 \subset G_2$, where G_2 is a larger Lie group. The deformation problem amounts to finding and studying discrete embeddings $\rho_s : \Gamma \to G_2$, which extend ρ_0.

When Γ is the fundamental group of a surface, $G_1 = \mathrm{Is}(\boldsymbol{H}^2)$, the isometry group of the hyperbolic plane, and $G_2 = \mathrm{Is}(\boldsymbol{H}^3)$, the isometry group of hyperbolic three space, one is dealing with the theory of quasifuchsian groups, which is quite well developed. (See, for instance, the bibliography in [**T**].)

The *complex hyperbolic plane* $\boldsymbol{CH}^2$ is a 2 complex dimensional manifold, which is negatively curved, Kähler, and also a symmetric space. It contains

* Supported by a National Science Foundation Research Grant and an Alfred P. Sloan Research Fellowship.

$\boldsymbol{H}^2$ as a totally real, totally geodesic subspace, and is often considered to be its complexification. The theory of deforming $\mathrm{Is}(\boldsymbol{H}^2)$ representations into $\mathrm{Is}(\boldsymbol{CH}^2)$ is also quite rich, though much less developed. (For a representative sample of such work, see [**FZ**], [**GKL**], [**GuP**], [**KR**], [**Tol**].)

1.1 The Goldman Parker Conjecture

In [**GP**], Goldman and Parker took one of the first steps on the road to a theory of complex hyperbolic quasifuchsian groups. They defined and partially classified the *complex hyperbolic ideal triangle groups*, which are representations $\rho_s : \Gamma \to \mathrm{Is}(\boldsymbol{CH}^2)$. Here Γ is the free product $\boldsymbol{Z}/2 * \boldsymbol{Z}/2 * \boldsymbol{Z}/2$. The representation ρ_s maps the standard generators of Γ to distinct order two *complex reflections*, such that any product of two distinct generators is parabolic. A complex reflection is an isometry which has, for a fixed point set, a complex line in $\boldsymbol{CH}^2$. (See §2.3 for more information.)

Modulo conjugation, there is a one parameter family $\{\rho_s |\ s \in \boldsymbol{R}\}$ of such representations. The indexing parameter, s, is the tangent of the *angular invariant* of the ideal triangle formed by the 3 complex lines fixed by the generators. The angular invariant measures the extent to which the vertices of the triangle fail to lie in a totally real subspace. (See §2.5 for a definition.) The representation ρ_0 is the complexification the familiar *real ideal triangle group* generated by reflections in the sides of an ideal triangle in $\boldsymbol{H}^2$.

Let $\underline{s} = (105/3)^{1/2}$ and $\overline{s} = (125/3)^{1/2}$. According to Goldman-Parker:

Theorem [GP]: *If $|s| > \overline{s}$ then ρ_s is not a discrete embedding. If $|s| \leq \underline{s}$ then ρ_s is a discrete embedding.*

Here is a sketch of the first half of this result. Let g_s be the product of all three generators of $\rho_s(\Gamma)$, taken in any order. In [**GP**] it is shown that g_s is loxodromic for $|s| \in [0, \overline{s})$, parabolic for $|s| = \overline{s}$, and elliptic for $|s| > \overline{s}$. (See §2.1 for a classification of isometries.) If g_s is elliptic, with finite order, then ρ_s is not an embedding. If g_s is elliptic, with infinite order, then ρ_s is not discrete.

The theorem above is not sharp. For $|s| > \underline{s}$ the analysis in [**GP**] breaks down, but Goldman and Parker conjecture that ρ_s remains a discrete embedding for $|s| \in (\underline{s}, \overline{s}]$. The significance of the result/conjecture combination is that it proposes the first complete description of a complex hyperbolic deformation problem.

1.2 Results and Methods

The purpose of this paper is to prove a sharp version of Goldman-Parker conjecture.

Main Theorem: *ρ_s is a discrete embedding if and only if g_s is not elliptic. Also, ρ_s is indiscrete if g_s is elliptic.*

Our indiscreteness proof uses some Galois theory to show that g_s must have infinite order when it is elliptic.

For our discreteness proof, let $\Gamma_s = \rho_s(\Gamma)$. Let $\partial \boldsymbol{CH}^2$ be the ideal boundary of $\boldsymbol{CH}^2$. We construct a surface-like set $\boldsymbol{Z}(s) \subset \partial \boldsymbol{CH}^2$, which we call a *dented torus*. We then prove that the orbit $\Gamma_s \boldsymbol{Z}(s)$ consists of (essentially) disjoint surface-like sets. This phenomenon feeds into a variant of the Klein combination theorem to prove that ρ_s is a discrete embedding.

We found $\boldsymbol{Z}(s)$ experimentally, using our interactive program [**S1**]. The technical part of this paper consists in making the pictures in [**S1**] into rigorous proofs, via computation and numerical analysis. While our proof is logically independent from [**S1**], most of the ideas came from analyzing the output of this program.

We use two kinds of programs to verify our computational claims. The first program, which computes quantities depending the eigenvalues of g_s, is Mathematica code [**M**]. This code runs with much more precision than we need. The second program, which is used for the bulk of the computation, is C code [**KeR**]. Our C code uses only those operations which conform to the IEEE standards [**I**] and employs interval arithmetic to rigorously bound the roundoff errors. Our code takes about 350 computational hours, when run on a Sparc Ultra 5. We ran the code, in parallel, on 11 such machines, over the course of a weekend.

Our code includes a variety of interactive visual displays, which allow the user to see, to a large extent, that everything operates as claimed. The code is available upon request.

We give explicit parametrizations of the main objects in the paper, as well as pseudocode expositions of the main algorithms. We hope this is enough information for the inclined (and energetic) reader to reproduce the results here in an independent experiment.

1.3 Overview

In §2 we review some basic complex hyperbolic geometry.

In §3 we define the triangle groups, establish the indiscreteness part of our main theorem, and study the eigenvalues of g_s.

In §4, we study the action of Γ_s on the *Clifford torus*,

$$T = \{(z,w) \in \boldsymbol{C}^2 |\ |z| = |w| = \sqrt{2}/2\} \subset S^3.$$

(The ideal boundary of $\boldsymbol{CH}^2$ can be naturally identified with the three sphere.) We give an alternate proof of the Goldman-Parker discreteness result. Though our proof breaks down at the same place the proof in [**GP**] breaks down, it sheds new light on what should be done in the critical interval $(\underline{s}, \overline{s}]$. Our basic idea is to put some dents in the Clifford torus, so that the resulting surface moves around better under the action of the group.

In §5-6 we construct the "surfaces" which replace the Clifford torus. In §5, we introduce a projectively natural coning operation, the *hybrid cone construction*. This procedure creates surfaces called *hybrid sectors*, which are certain embedded solid triangles. In §6 we introduce, for each parameter s, the dented torus, $\boldsymbol{Z}(s)$, a surface which is made from cutting out two solid triangles from the Clifford torus and gluing back 6 hybrid sectors.

In §7-9 we give the bulk of the proofs. In §7 we give the discreteness proof of the Main Theorem for the parameter $\overline{s}$, modulo two technical estimates, Estimates 1 and 2. In §8 we establish the Year Lemma, a result which shows that we only need consider 365 parameters in the interval J. In §9 we give the general discreteness proof, modulo the two estimates, Estimates 1 and 2.

The remainder of the paper is devoted to establishing and illustrating Estimates 1 and 2. In §10 we describe the method by which we estimate the location of a hybrid sector in space using finitely many computations. In §11 we detail the computation scheme used to verify Estimates 1 and 2. In §12 we discuss the implementation and computational accuracy of our code. We also give a record of the actual calculations. In §13 we illustrate Estimates 1 and 2 with computer plots, produced with our code.

Suggested Reading: We have indicated, through a series of remarks, the material in §2-6 which is strictly necessary for the proof of the parabolic case. Read only this material, and then read §7. Following this, skip to §13, and look at the computer pictures, which give compelling evidence that Estimates 1 and 2 are true. Afterwards, try to understand the general case.

1.4 Related Results

This paper is the first in a series of results. We prove in [**S2**] that the orbifold at infinity, in the parabolic case, is commensurable to the Whitehead link complement. [**S2**] also gives a noncomputational proof that there is some $\epsilon > 0$ such that ρ_s is a discrete embedding for $s \in (\overline{s} - \epsilon, \overline{s}]$.

In [**S3**] we explain (among other things) how to build models, out of string, of the limit sets of the complex hyperbolic ideal triangle groups.

In [**S4**] we consider an extremely deformed discrete representation of the $(4, 4, 4)$-Hecke triangle group, and use it to produce the first example of a closed hyperbolic 3-manifold which bounds a complex hyperbolic 4-manifold.

For some neat results and conjectures on the algebraic side of the complex hyperbolic ideal triangle groups see [**Sa**].

For deformations of other triangle groups into $PU(2, 1)$, see [**W-G**].

For another example of an application of computation to hyperbolic geometry, which is independent from ours, see the monumental [**GMT**].

1.5 Acknowledgements

I must say that writing this paper has been an extremely gruelling experience, though sometimes an exhilarating one. I would like to thank Bill Goldman for his perspective and encouragement as well as for the efficient proof of Lemma 2.2. I would like to thank Martin Bridgeman, Peter Doyle, Jeremy Kahn, Josh Maher, Andy Mayer, Robert Miner, Robert Meyerhoff, John Parker, Bill Thurston, and Justin Wyss-Gallifent for interesting conversations relating to this work. I would like to thank the tireless referees for many helpful stylistic suggestions. Finally, I would like to thank my wife Brienne Brown for her C programming advice, and in particular for suggesting the elegant subdivision algorithms used in §10.8 and §11.1.

I dedicate this paper to my daughter, Lucina Caroline Schwartz, who was born right around the time I started thinking about triangle groups, and who is now learning about triangles herself. I also dedicate this paper to the memory of Hanna Sandler, a great enthusiast for the complex hyperbolic triangle groups, who passed away this winter.

2 Background

2.1 The Complex Hyperbolic Plane

$\boldsymbol{C}^{2,1}$ is a copy of the vector space $\boldsymbol{C}^3$ equipped with the Hermitian form

$$\langle u, v\rangle = u_1\overline{v}_1 + u_2\overline{v}_2 - u_3\overline{v}_3 \tag{1}$$

The spaces $\boldsymbol{CH}^2$ and $\partial\boldsymbol{CH}^2$ are respectively the projective images, in the complex projective plane $\boldsymbol{CP}^2$, of

$$N_- = \{v \in \boldsymbol{C}^{2,1} |\ \langle v, v\rangle < 0\}; \quad N_0 = \{v \in \boldsymbol{C}^{2,1} |\ \langle v, v\rangle = 0\} \tag{2}$$

(See [**G**, p.67] or [**E**].) The map

$$\Theta(v_1, v_2, v_3) = \left(\frac{v_1}{v_3}, \frac{v_2}{v_3}\right) \tag{3}$$

takes N_- and N_0 respectively to the open unit ball and unit sphere in $\boldsymbol{C}^2$. Henceforth we identify $\boldsymbol{CH}^2$ with the open unit ball.

Given a point $V \in \boldsymbol{CH}^2 \cup S^3$, we will say that $\tilde{V} \in \Theta^{-1}(V)$ is a *lift* of V and that a lift of the form $(v_1, v_2, 1)$ is *affinely normalized*. We define the *vector* $\Theta^{-1}(V)$ as the affinely normalized lift of V.

$SU(2,1)$ is the group of $\langle , \rangle$ preserving, determinant 1 complex linear transformations. $PU(2,1)$ is the projectivization of $SU(2,1)$, and elements of $PU(2,1)$ preserve $\boldsymbol{CH}^2$. Concretely, each $\tilde{T} \in SU(2,1)$ determines an element of $PU(2,1)$ via

$$T = \Theta \circ \tilde{T} \circ \Theta^{-1}. \tag{4}$$

The map $\tilde{T} \to T$ is a $3-1$ surjective lie group homomorphism.

An element $T \in PU(2,1)$ is called *loxodromic* if T has exactly 2 fixed points in S^3, *parabolic* if it has exactly one fixed point in S^3, and *elliptic* if it has a fixed point in $\boldsymbol{CH}^2$. This classification is exhaustive and exclusive. T is called *ellipto-parabolic* if T is parabolic and also stabilizes a complex line in $\boldsymbol{CP}^2$. (See [**G**, p.203] more details.) For instance, the element $g_{\overline{s}}$ is ellipto-parabolic.

$\boldsymbol{CH}^2$ has a $PU(2,1)$-invariant Riemannian metric, unique up to scale. Let δ denote the path metric induced by this Riemannian metric. When normalized as on [**G**, p. 78] we have

$$\cosh^2 \frac{\delta(v,w)}{2} = \frac{\langle \tilde{v}, \tilde{w}\rangle\langle \tilde{w}, \tilde{v}\rangle}{\langle \tilde{v}, \tilde{v}\rangle\langle \tilde{w}, \tilde{w}\rangle} = \hat{\delta}(v,w). \tag{5}$$

2.2 Heisenberg Space

Let $\Re(z)$ and $\Im(z)$ denote the real and imaginary parts of a complex number z. The *Siegel domain* is the affine subset

$$\{(z,w)|\ \Re(w) > |z|^2\} \subset \boldsymbol{C}^2 \subset \boldsymbol{CP}^2 \tag{6}$$

Let $\mathcal{H}$ stand for $\boldsymbol{C} \times \boldsymbol{R}$. We call $\mathcal{H}$ *Heisenberg space*. Given $p \in S^3$, a *Heisenberg stereographic projection from* p is a map $\boldsymbol{B} : S^3 - \{p\} \to \mathcal{H}$ which has the form $\boldsymbol{B} = \pi \circ \beta$. Here $\pi(z,w) = (z, \Im(w))$ and β is a complex projective transformation of $\boldsymbol{CP}^2$ which identifies $\boldsymbol{CH}^2$ with the Siegel domain. We write $\infty = \boldsymbol{B}(p)$ in this case. For instance

$$\boldsymbol{B}_0(z,w) = \left(\frac{w}{1+z}, \Im\frac{1-z}{1+z}\right) \tag{7}$$

is a Heisenberg stereographic projection which maps $(-1,0)$ to ∞. The map $\boldsymbol{B}_0$ is a close relative of the *Cayley Transform* given on [**G**, p. 112]. The map $\boldsymbol{B}_0$ conjugates the $PU(2,1)$ stabilizer of $(-1,0)$ to certain affine maps of $\mathcal{H}$.

We call $E_0 = \{0\} \times \boldsymbol{R}$ the *center* of Heisenberg space.

The complex lines tangent to S^3 form a canonical contact distribution on S^3. We call this distribution $\mathcal{E}$. Heisenberg stereographic projection maps $\mathcal{E}$ to a corresponding distribution in $\mathcal{H}$, which we give the same name. In $\mathcal{H}$, the distribution $\mathcal{E}$ is the null distribution to the contact form

$$\omega = 2ydx - 2xdy + dt \tag{8}$$

(See [**G**, p. 124].) In this formula, $\boldsymbol{C}$ has been identified with $\boldsymbol{R}^2$ in the usual way. $\mathcal{E}$ has cylindrical symmetry. It is preserved under maps of the form

$$(z,t) \to (\lambda z, |\lambda|^2 t + r); \quad \lambda \in \boldsymbol{C}^*,\ r \in \boldsymbol{R}.$$

If Π is a plane in $\mathcal{E}$, based at the point (z,t), then the maximum slope of a vector in Π is $2|z|$.

We say that a curve, in either S^3 or $\mathcal{H}$, is $\mathcal{E}$-*integral* if its tangent vector, at every point, is contained in $\mathcal{E}$. The term $\mathcal{E}$-*integral* is sometimes called *CR horizontal*. We prefer to use the former term, because the term *horizontal* comes up elsewhere in the paper.

2.3 C-Circles

A *complex slice* is the intersection of a complex line in $\boldsymbol{C}^2$ with $\boldsymbol{CH}^2$. Complex slices are totally geodesic subspaces, when considered as Riemannian subspaces of $\boldsymbol{CH}^2$. A $\boldsymbol{C}$*-circle* (also known as a *chain*) is the intersection of a complex line with S^3, provided this intersection is more than a single point. A $\boldsymbol{C}$-circle is a round circle, transverse to $\mathcal{E}$. A $\boldsymbol{C}$*-arc* is a nontrivial arc of a $\boldsymbol{C}$-circle. Given two points $p \neq q \in S^3$, there is a unique $\boldsymbol{C}$-circle containing p and q.

Here is a method for parametrizing $\boldsymbol{C}$-arcs. Suppose X, Y, Z are three distinct points contained in a common $\boldsymbol{C}$-circle, C. After switching the order of X and Y if necessary, there are lifts $\tilde{X}, \tilde{Y}, \tilde{X}$, unique up to multiplying all three vectors by the same unit complex number, such that

$$\langle \tilde{X}, \tilde{Y} \rangle = i; \quad \langle \tilde{X}, \tilde{Z} \rangle = \langle \tilde{Y}, \tilde{Z} \rangle = 1 \tag{9}$$

(Compare §2.5 below.) Note that $i\tilde{X} + t\tilde{Z} \in N_0$ for $t \in \boldsymbol{R}$, so that

$$C_Z(X, Y; t) = \Theta(i\tilde{X} + t\tilde{Z}); \quad t \in [0, 1]. \tag{10}$$

parametrizes the $\boldsymbol{C}$-arc of C which joins X to Y and which avoids Z.

Let $N_+ = \boldsymbol{C}^{2,1} - N_- - N_0$. If C is a $\boldsymbol{C}$-circle, then there is the *polar vector* $C^* \in N_+$, unique up to scaling, such that $C = \{v \in N_0 |\ \langle v, C^* \rangle = 0\}$. There is a unique involution $I_C \in PU(2,1)$ fixing C. This map is computed by setting $I_C = \Theta \circ I_{C^*} \circ \Theta^{-1}$, where

$$I_{C^*}(\tilde{u}) = -\tilde{u} + \frac{2\langle \tilde{u}, C^* \rangle}{\langle C^*, C^* \rangle} C^*. \tag{11}$$

(See [**G**, p. 70].) Another feature of the polar vector is this: Two $\boldsymbol{C}$-circles, C_1 and C_2 are linked in S^3 iff $\hat{\delta}(C_1^*, C_2^*) < 1$, where $\hat{\delta}$ is as in Equation 5.

We say that a *Heisenberg chain* is the image of a chain under a Heisenberg stereographic projection. Curves of the form $(\{z\} \times \boldsymbol{R}) \cup \infty$ are chains. In particular, the center of $\mathcal{H}$ is a chain (with ∞ deleted.) All other Heisenberg chains are ellipses which project to round circles under the projection $\pi_{\boldsymbol{C}} : \mathcal{H} \to \boldsymbol{C}$. (See [**G**, p.125].) Let C be such a chain, with center of mass m. Let E_m be the plane of $\mathcal{E}$ based at m. Let $\hat{E}_m$ be the affine plane which is tangent to E_m at m. We call $\hat{E}_m$ the *prolongation* of E_m. We have $C \subset \hat{E}_m$. We will say that a *round* Heisenberg chain is one which is, itself, a round circle. The center of mass of a round Heisenberg chain is contained in the center of $\mathcal{H}$. Such curves are contained in planes of the form $\boldsymbol{C} \times \{t\}$.

2.4 $\boldsymbol{R}$-circles

A *real slice* is a totally real, totally geodesic subspace of $\boldsymbol{CH}^2$. Every real slice is isometric to the real slice $\boldsymbol{R}^2 \cap \boldsymbol{CH}^2$. An $\boldsymbol{R}$-circle is the accumulation set, in S^3, of a real slice. Every $\boldsymbol{R}$-circle is $PU(2,1)$-equivalent to the particular $\boldsymbol{R}$-circle $\boldsymbol{R}^2 \cap S^3$. All $\boldsymbol{R}$-circles are $\mathcal{E}$-integral.

We say that an $\boldsymbol{R}$-circle is *round* if it is a round circle. An $\boldsymbol{R}$-circle is round iff the real slice containing it lies in a real 2-plane in $\boldsymbol{C}^2$, which is true iff the real slice contains $(0,0)$. The geodesics in a round $\boldsymbol{R}$-circle are line segments in $\boldsymbol{C}^2$. Not all $\boldsymbol{R}$-circles are round. An $\boldsymbol{R}$-*arc* is a nontrivial arc of an $\boldsymbol{R}$-circle. There is an S^1-family of $\boldsymbol{R}$-arcs containing two points $p \neq q \in S^3$. The union of all such arcs is called a *spinal sphere*. (See [**G**, p.152].)

Here is a method for parametrizing $\boldsymbol{R}$-arcs. Suppose X, Y, Z are three distinct points contained in a common $\boldsymbol{R}$-circle, R. There are lifts $\tilde{X}, \tilde{Y}, \tilde{X}$, unique up to scaling all three vectors by the same complex number, such that

$$\langle \tilde{X}, \tilde{Y} \rangle = \langle \tilde{Y}, \tilde{Z} \rangle = \langle \tilde{Z}, \tilde{X} \rangle \in \boldsymbol{R}. \tag{12}$$

(Compare §2.5 below.) We call $\{\tilde{X}, \tilde{Y}, \tilde{Z}\}$ an *equalized choice* of lifts. The curve

$$R_Z(X, Y; u) = \Theta((1-u)\tilde{X} + u\tilde{Y} + u(u-1)\tilde{Z}); \quad u \in [0,1] \tag{13}$$

parametrizes the $\boldsymbol{R}$-arc of R which joins X to Y, but which avoids Z.

We say that a *Heisenberg* $\boldsymbol{R}$*-circle* is the image of an $\boldsymbol{R}$-circle under a Heisenberg stereographic projection. Any Heisenberg $\boldsymbol{R}$-circle γ which contains ∞ is (the extension of) a straight line. We call these $\boldsymbol{R}$-circles *straight*. γ has the form $(L \times \{t\}) \cup \infty$ where $L \in \boldsymbol{C}$ is a line through the origin, if and only if γ is straight and intersects the center of $\mathcal{H}$. In this case we call γ *level*. All other Heisenberg $\boldsymbol{R}$-circles are curves, which project to lemniscates via the projection $\pi_{\boldsymbol{C}}$. (See [**G**, p.139].)

Here is a geometric interpretation of our parametrization.

Lemma 2.1 *Let $\boldsymbol{B}_0$ be as in Equation 7. If $Z = (-1, 0)$ and X, Y, Z lie on a common $\boldsymbol{R}$-circle then $\boldsymbol{B}_0(R_Z(X, Y; u)) = (1-u)\boldsymbol{B}_0(X) + u\boldsymbol{B}_0(Y)$*

Proof: Since $\boldsymbol{B}_0$ maps the $\boldsymbol{R}$-circle containing X, Y, X to a straight line, the point $P = \boldsymbol{B}_0(R_Z(X, Y; u))$ must be a convex combination of $\boldsymbol{B}_0(X)$

and $\boldsymbol{B}_0(Y)$. Our parametrization of $\boldsymbol{R}$-arcs is natural in the following sense: If, for $j = 1, 2$, the points X_j, Y_j, Z_j are contained on an $\boldsymbol{R}$-circle, then an element of $PU(2,1)$ which carries $\{X_1, Y_1, Z_1\}$, in order, to $\{X_2, Y_2, Z_2\}$, also carries $R_{Z_1}(X_1, Y_1; u)$ to $R_{Z_2}(X_2, Y_2; u)$. Also, $\boldsymbol{B}_0$ conjugates the stabilizer of $Z = (-1, 0)$ to affine maps of $\mathcal{H}$. The facts just mentioned imply that the particular convex combination depends only on u, and not on the triple of points chosen.

We will make the computation for the points $X = (1, 0)$ and $Y = (0, 1)$ and $Z = (-1, 0)$ an equalized choices of lifts is $\tilde{X} = (1, 0, 1)$ and $\tilde{Y} = (0, 2, 2)$ and $\tilde{Z} = (-1, 0, 1)$. Equation 13 gives

$$R_Z(X, Y; u) = \Big(\frac{1 - u^2}{1 + u^2}, \frac{2u}{1 + u^2}\Big)$$

We have $\boldsymbol{B}_0(X) = (0, 0)$ and $\boldsymbol{B}_0(Y) = (1, 0)$ and, from the calculation above, $\boldsymbol{B}_0(P) = u$. Since the result is true in this case, it is true in all cases. ♠

2.5 The Angular Invariant

See [**G**, pp. 210-214] for proofs of everything in this section.

Given three points $X \neq Y \neq Z \in S^3$, the *Cartan angular invariant* is

$$\boldsymbol{A}(X, Y, Z) = \arg[-\langle \tilde{X}, \tilde{Y}\rangle\langle \tilde{Y}, \tilde{Z}\rangle\langle \tilde{Z}, \tilde{X}\rangle] \in [-\frac{\pi}{2}, \frac{\pi}{2}]. \tag{14}$$

We have $\boldsymbol{A}(X, Y, Z) = \pm\pi/2$ iff these points lie in a common $\boldsymbol{C}$-circle, and $\boldsymbol{A}(X, Y, Z) = 0$ iff these points lie in a common $\boldsymbol{R}$-circle.

2.6 The Group Law on S^3

Recall that S^3 is a Lie group. Thinking of S^3 as the unit sphere in $\boldsymbol{C}^2$, as above, the group law on S^3 is

$$(z_1, w_1) \cdot (z_2, w_2) = (z_1 w_1 - z_2 \overline{w}_2, z_1 w_2 + z_2 \overline{w}_1). \tag{15}$$

The right multiplication map $R_X(Y) = Y \cdot X$ is an element of $PU(2,1)$ which acts isometrically on S^3, in the round metric, and moves all points by the same amount. The point here is that R_X commutes with the complex structure, which is left multiplication by i.

2.7 The Clifford Torus

We do not know a reference for the material in this section.

The *Clifford torus* is the torus $T = \{(z,w)|\ |z| = |w| = \sqrt{2}/2\} \subset S^3$. Define $\arg : T \to T_0$ by the formula $\arg(z,w) = (\arg z, \arg w)$. The preimages, under arg, of curves of slope 0 ,1 and ∞ are all chains on T. We call such chains, respectively, *horizontal*, *vertical*, and *diagonal*. The preimages, under arg, of curves of slope -1 are round $\boldsymbol{R}$-circles on T, having the form $\{(z,w)|\ zw = \lambda\} \cap S^3$, where $|\lambda| = 1$.

We say that a *Clifford triangle* is a solid triangle in T whose edges are contained in chains, one from each of the three foliations. See Figure 3.1 for an example.

We say that a *Clifford rectangle* is a solid rectangle whose boundary consists of two vertical $\boldsymbol{C}$-arcs and two horizontal $\boldsymbol{C}$-arcs. In parametrizing a Clifford rectangle we wish to avoid the exponential function, for computational reasons. Here is how we do it. Let Q be a Clifford rectangle. Let H and V be maximal horizontal and vertical $\boldsymbol{C}$-arcs in ∂Q.

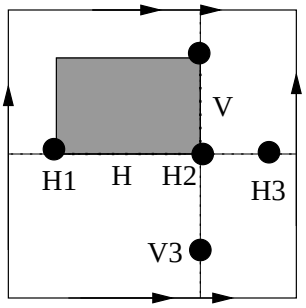

Figure 2.6

Let H_1 and H_2 be the endpoints of H and let H_3 be the midpoint of $\check{H} - H$. Here $\check{H}$ is the $\boldsymbol{C}$-circle containing H. Likewise define V_1, V_2 and V_3. We parametrize Q by

$$Q(t,u) = (\pi_1(C_{H_3}(H_1, H_2; t)), \pi_2(C_{V_3}(V_1, V_2; u))). \tag{16}$$

Here π_1 and π_2 are projections onto the first and second factors, and the components of our parametrization come from Equation 10.

We call this the *rational parametrization* of Q. It appears that there are two choices for H and two for V. However, recall from our definition of $C_{H_3}(H_1, H_2; t)$ that the points H_1, H_2, H_3 must be correctly ordered. Likewise for V_1, V_2, V_3. These extra constraints make the rational parametrization unique.

2.8 Pure Translation Flows

Remark: The reader interested only in the parabolic case of the main theorem can skip this section.

Say that a *pure translation* along a geodesic $\gamma \in \boldsymbol{CH}^2$ is one which preserves all real slices containing γ. Say that a *pure translation flow* along γ is a flow $\phi_t : \boldsymbol{CH}^2 \to \boldsymbol{CH}^2$ such that ϕ_t is a pure translation of γ, for all t. Let I be the geodesic $(-1,1) \times \{0\}$. Let $\| \ \|$ be the Euclidean norm on $\boldsymbol{C}^2$.

Lemma 2.2 *The vector field $V(z,w) = (1-z^2, zw)$ generates a pure translation flow along I.*

Proof: Let $\boldsymbol{B}_0$ be the map defined in Equation 7. Let $(\zeta, \omega) = \boldsymbol{B}_0(z,w)$. We compute

$$d\boldsymbol{B}_0(V) = \begin{bmatrix} -\frac{w}{(1+z)^2} & \frac{1}{1+z} \\ \frac{-2}{(1+z)^2} & 0 \end{bmatrix} \begin{bmatrix} z^2-1 \\ zw \end{bmatrix} = (\frac{w}{z+1}, \frac{2-2z}{1+z}) = (\zeta, 2\omega).$$

This vector field generates the flow $\psi_r(\zeta,\omega) = (r\zeta, r^2\omega)$. Clearly, ψ_r is a flow by complex linear maps which preserves the Siegel domain. Hence, ϕ_t is a flow by complex hyperbolic isometries, obviously preserving I and $\boldsymbol{R}^2$. ♠

Lemma 2.3 *Suppose that $\hat{R}$ is a real 2-plane which contains $(0,0)$. Suppose $p_1, p_2 \in \hat{R} - \boldsymbol{CH}^2 - S^3$ are two points such that $(0,0), p_1, p_2$ are all contained on a line $L \subset \hat{R}$. Let β be the pure translation along $L \cap \boldsymbol{CH}^2$ such that $\beta(p_1) = p_2$. Then, for all $q \in S_3$,*

$$\rho(q, \beta(q)) \leq \frac{\|p_1 - p_2\|}{S^2 - 1}; \quad S = \inf(\|p_1\|, \|p_2\|).$$

Proof: The stabilizer subgroup of $(0,0)$ in $PU(2,1)$ acts isometrically on S^3 and transitively permutes the real 2-planes through $(0,0)$, as well as the real lines through $(0,0)$. Thus, we may assume that $\hat{R} = \boldsymbol{R}^2$, that $L = I$, that $p_1 = (x_1, 0)$ and $p_2 = (x_2, 0)$, with $1 < x_1 < x_2 < \infty$. Let V be the vector field from Lemma 2.2. Since $\sup_{x \in S^3} \|V(x)\| = 1$, we conclude that $\rho(q, \phi_t(q)) \leq t$ for all $q \in S^3$. The value of t, for which $\phi_t(p_1) = p_2$, is

$$t = \int_{x_1}^{x_2} \frac{dx}{x^2 - 1} \leq \frac{x_2 - x_1}{x_1^2 - 1} = \frac{\|p_1 - p_2\|}{S^1 - 1}.$$

♠

3 The Triangle Groups

3.1 Basic Definitions

Given $s \in [0, \infty)$ let Δ_s be the Clifford triangle having vertices

$$(\beta_s, \beta_s); \quad (\beta_s, \overline{\beta}_s); \quad (\overline{\beta}_s, \overline{\beta}_s); \qquad \beta_s = \frac{(s+i)}{\sqrt{2+2s^2}}. \tag{17}$$

The angular invariant of these three points is $\pm \arctan s$, depending on the order in which they are taken. The first part of Figure 3.1 shows the images of these points under the arg map.

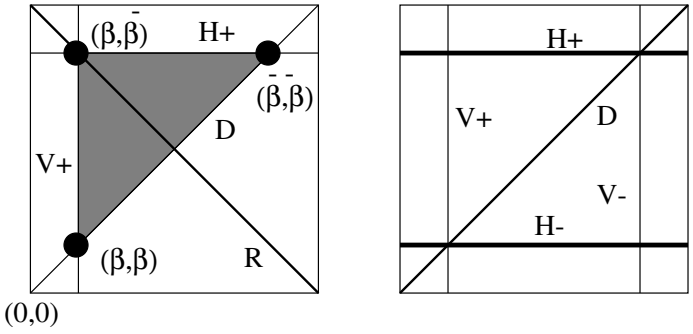

Figure 3.1

Let $H_{+,s}$, $V_{+,s}$ and D be the horizontal, vertical, and diagonal $\boldsymbol{C}$-circles containing pairs of these points. Let R be the $\boldsymbol{R}$-circle which bisects Δ_s. Define

$$d(z,w) = (w,z); \quad r(z,w) = (\overline{w}, \overline{z}). \tag{18}$$

Note that d is the complex reflection fixing D and r is an antiholomorphic involution fixing R. Note that d and r commute.

We define $H_{-,s} = d(r(H_{+,s}))$ and $V_{-,s} = d(r(V_{+,s}))$. The second part of Figure 3.1 shows these chains. Let $h_{\pm,s}$ be the complex reflection fixing $H_{\pm,s}$, etc. The group $\Gamma_s = \rho_s(\Gamma)$ is generated by the triple $\{d, h_{+,s}, h_{-,s}\}$. We define

$$g_s = h_{+,s} \circ h_{-,s} \circ d \tag{19}$$

Since r conjugates $h_{\pm,s}$ to $v_{\pm,s}$ and vice versa, we have

$$r\Gamma_s r^{-1} = \Gamma_s; \quad rg_s r^{-1} = g_s^{-1} \tag{20}$$

The representations ρ_s and ρ_{-s} have the same image in $PU(2,1)$, so we are justified in taking $s \in [0, \infty)$. We define $J = [\underline{s}, \overline{s}]$. Usually we take $s \in J$.

3.2 Matrices

We now give formulas for $SU(2,1)$ lifts of some of the elements defined above.

$$\tilde{h}_{+,s} = \begin{bmatrix} -1 & 0 & 0 \\ 0 & 3 & -4\overline{\beta}_s \\ 0 & 4\beta_s & -3 \end{bmatrix}; \quad \tilde{h}_{-,s} = \begin{bmatrix} -1 & 0 & 0 \\ 0 & 3 & -4\beta_s \\ 0 & 4\overline{\beta}_s & -3 \end{bmatrix}. \tag{21}$$

$$\tilde{d} = \begin{bmatrix} 0 & -1 & 0 \\ -1 & 0 & 0 \\ 0 & 0 & -1 \end{bmatrix}; \tag{22}$$

Setting $\tilde{g} = \tilde{h}_+ \tilde{h}_- \tilde{d}$, we have

$$\tilde{g}_s = \begin{bmatrix} 0 & -1 & 0 \\ -A_1(s) & 0 & A_2(s) \\ -A_2(s) & 0 & -\overline{A}_1(s) \end{bmatrix}; \quad A_1(s) = \frac{s+17i}{s+i}; \quad A_2(s) = \frac{12\sqrt{2}i}{\sqrt{1+s^2}}. \tag{23}$$

Clearly, $\tilde{d}$ is a lift of the map $d(z,w) = (w,z)$. One can check easily that $\tilde{h}_{\pm,s}$ is a determinant one involution which preserves $N_0 \subset \boldsymbol{C}^{2,1}$. One can also check that this matrix has, as an eigenvector, a vector which is polar to $H_{\pm,s}$. One can also take traces of these matrices and their products, checking that they agree with the traces of the corresponding matrices in [**GP**].

3.3 Indiscreteness Proof

We now show that ρ_s is indiscrete for $s \in (\overline{s}, \infty)$. The work in [**GP**] shows that g_s is elliptic for such s. We will show that g_s has infinite order.

From the formula for $\tilde{g}_s$, we see that the trace τ_s of $\tilde{g}_s$ satisfies the equation

$$(\tau_s + N + 1)(\overline{\tau}_s + N + 1) = N^2; \quad \tau_s \neq -1 \tag{24}$$

for $N = 8$. Note that $\Re(\tau_s) < -1$ as long as $N \in \boldsymbol{N}$. If g_s has finite order then

$$\tau_s = \omega_n^p + \omega_n^q + \omega_n^r; \quad \omega_n = \exp(2\pi i/n); \quad p+q+r = 0. \tag{25}$$

Here n is taken as small as possible. Obviously $n > 2$. We suppose that Equations 24 and 25 are true for some $N \in \boldsymbol{N}$, and derive a contradiction. We set $\tau = \tau_s$.

Lemma 3.1 *n divides 12.*

Proof: For k relatively prime to n, let $\sigma_k : \boldsymbol{Q}[\omega_n] \to \boldsymbol{Q}[\omega_n]$ be the Galois automorphism determined by $\sigma_k(\omega_n) = \omega_n^k$. Equation 24 is defined in $\boldsymbol{Q}[\omega_n]$, so it remains true if we replace τ by $\sigma_k(\tau)$. In particular, $\Re(\sigma_k(\tau)) < -1$. Summing over all those $k \in \{1, ..., n-1\}$ which are relatively prime to n, we get $\Re(\sum_k \sigma_k(\tau)) < -\phi(n)$. Here ϕ is the Euler phi function. Hence

$$|\sum_k \sigma_k(\tau)| > \phi(n). \tag{26}$$

For $m = p, q, r$ let (m, n) be the greatest common divisor of m and n. Let $d_m = n/(m, n)$. Note ω_n^m is a primitive d_mth root of unity, and the sum of all such roots one of $-1, 0, 1$. The map $\boldsymbol{Z}/n \to \boldsymbol{Z}/d_m$ induces a map $(\boldsymbol{Z}/n)^* \to (\boldsymbol{Z}/d_m)^*$, which is onto, with multiplicity $\phi(n)/\phi(d_m)$. Hence

$$|\sum_k \sigma_k(\omega_n^m)| \le \frac{\phi(n)}{\phi(d_m)}. \tag{27}$$

Combining Equations 25, 26 and 27 we get

$$\frac{1}{\phi(d_p)} + \frac{1}{\phi(d_q)} + \frac{1}{\phi(d_r)} > 1. \tag{28}$$

There is no positive integer k such that $\phi(k) = 3$, and $\phi(k) = 2$ only for $k \in \{2, 3, 4, 6\}$. We conclude that all three roots are 12th roots of unity. ♠

Remark: For each choice of N, Lemma 3.1 leaves only finitely many cases to check. One can finish the proof, for small choices of N, by a quick computer search. We did this for $N = 8$, the case of interest. The argument following this remark finishes the proof, in all cases, in a noncomputational manner.

Lemma 3.2 *None of p, q, r is relatively prime to n.*

Proof: Suppose that p is relatively prime to n. All our congruences will be taken mod n. Applying a Galois automorphism of $\boldsymbol{Q}[\omega_n]$ we arrange that $p = 1$. Assume first that n is even. Since $\Re(\tau) < -1$ we must have $\Re(\omega_n^q + \omega_n) < 0$ and $\Re(\omega_n^r + \omega_n) < 0$. This is only possible if $q, r \equiv n/2$. But then it is impossible to get $p + q + r = 0$. Similarly, if n is odd then $q, r \equiv (n \pm 1)/2$. Since $p+q+r = 0$, and $n > 2$ we must have $q \equiv r \equiv (n-1)/2$. Here $\omega^q = \omega^r$ is a primitive nth root of unity. We apply a second Galois automorphism to get $q = r = 1$. Thus $\Re(\omega^q + \omega^r) > 0$, a contradiction. ♠

Lemma 3.2 says, in particular, that n must have more than one prime factor. Thus, $n \in \{6, 12\}$. Suppose $n = 12$. Since $\omega_n^p \omega_n^q \omega_n^r = 1$, we see that d_r divides the least common multiple n' of d_p and d_q. Lemma 3.2 says $d_p, d_q, d_r < 12$. Suppose $n' < 12$. Since d_p, d_q, d_r all divide n' we can replace n by n', contradicting the minimality of n. Thus, $n' = 12$. Hence, (d_p, d_q) must be one of $(3,4)$, $(4,3)$, $(4,6)$ or $(6,4)$. From this it is easily seen that $d_r = 12$, a contradiction. The case $n = 6$ is similar.

Remark: The reader interested only in the parabolic case can skip to the next chapter at this point.

3.4 Near Monotonocity of the Eigenvector

Let E_s be the $\boldsymbol{C}$-circle stabilized by the element g_s, defined in §3.1. Let E_s^* be the affinely normalized vector which is polar to E_s. Note that E_s^* is an eigenvector corresponding to the norm one eigenvector λ_s of g_s. Since the element r conjugates g_s to g_s^{-1}, we have $E_s^* = (e(s), \overline{e}(s), 1)$.

Say that a function $f : J \to \boldsymbol{R}$ is *ϵ-monotone* if there is a monotone function $\tilde{f} : J \to \boldsymbol{R}$ such that $\|f - \tilde{f}\|_\infty \leq \epsilon$.

Lemma 3.3 (Near Monotonicity) *The functions* $\arg e(s)$ *and* $|e(s)|$ *are* 10^{-5}*-monotone decreasing for* $s \in J$.

Proof: We will show below that $|e'(s)| < 3$ for all $s \in J$. We explicitly evaluate the two functions above for 120001 maximally and evenly spaced points in J, and observe that the two functions are monotone decreasing on these points, up to a roundoff error of 10^{-20}. See §12 for details of the calculation. Using the bound on the derivative, together with the fact that J has length less than .54, we get the result of this lemma.

We turn now to our bound on $|e'(s)|$. Let A_1 and A_2 be the functions defined in §3.2. Let

$$X(s) = A_2(s)e(s) + \frac{\overline{e}(s)}{e(s)}.$$

We first establish the following implication:

$$|e(s)| < 1 \;\&\; |X(s)| > \frac{4}{3} \quad \Longrightarrow \quad |e'(s)| < 3 \;\&\; |X'(s)| < 20. \tag{29}$$

Assume that $|X| > 4/3$ and $|e| < 1$ at some parameter $s \in J$, which we suppress from our notation. Note that

$$\tilde{g}(e, \overline{e}, 1) = (\lambda_0 e, \lambda_0 \overline{e}, \lambda_0) = (-\overline{e}, -A_1 e + A_2, -A_2 e - \overline{A}_1).$$

Equating the first and third coefficients respectively gives

$$\lambda_0 = -\frac{\overline{e}}{e} \qquad e = \frac{-\overline{A}_1 - \lambda_0}{A_2}. \tag{30}$$

Combining these equations we obtain $A_2 e^2 + \overline{A}_1 e - \overline{e} = 0$. Differentiating with respect to s we get

$$[A_2' e^2 + \overline{A}_1' e] + (2A_2 e + \overline{A}_1)e' - \overline{e}' = 0.$$

Basic calculus shows that $|A_1'(s)|, |A_2'(s)| < .5$ for $s \in J$. If $|e| < 1$ then the bracketed expression above has norm less than 1. Therefore

$$|(2A_2 e + \overline{A}_1)e' - \overline{e}'| < 1 \tag{31}$$

Observe that

$$2A_2 e + \overline{A}_1 = A_2 e + \frac{A_2 e^2 + \overline{A}_1 e}{e} = A_2 e + \frac{\overline{e}}{e} = X.$$

Rearranging Equation 31 we arrive at

$$|e'(s)||X - u(s)| < 1; \qquad u(s) = e'(s)/\overline{e}'(s).$$

Since $u(s)$ is a unit complex number and $|X| > 4/3$ we see that $|X - u| > 1/3$. Hence $|e'| < 3$. Note that $|A_2(s)| < 3$ for $s \in J$. Hence

$$|X'| \le 2|A_2'||e| + 2|A_2||e'| + |\overline{A}_1'| < 1 + 18 + .5 < 20.$$

We now know that Equation 29 is true.

Say that $s \in J$ is a *good parameter* if the two bounds on the left hand side of Equation 29 hold at s. Otherwise say that s is a *bad parameter*. Let $s_0, ..., s_{55}$ be the set of 56 maximally and evenly spaced points in the interval J. Note that J has length $\sqrt{125/3} - \sqrt{35} < .55$. Thus, every point of J is within .005 of some point s_j. As explicit calculation shows that

$$|X(s_j)| > 1.49; \qquad |e(s_j)| < .9; \qquad j = 0, .., 10.$$

(See §12 for details of the calculation.) Suppose $s \in J$ is some bad parameter. Let s_j be the point in our list nearest to s. We can assume that all parameters in $[s_j, s]$ are good. This interval has length at most .005. Equation 29, says that $|X|$ and $|e|$ can each change by at most .1 on this interval. Hence, $|X(s)| \geq 1.49 - .1 > 1.3333...$ and $|e(s)| < .8 + .1 < 1$. This is a contradiction. Hence every parameter is good. Our bound follows immediately. ♠

4 Images of the Clifford Torus

4.1 A Discreteness Criterion

We begin with a discreteness criterion. This discreteness criterion is a close variant of the Ping-Pong Lemma and the Klein combination theorem. For original sources, see [**K**] and [**M2**]. A formulation which is similar to the one here appears in [**M1**].

Recall that $\rho_s : \Gamma \to PU(2,1)$ is our basic representation. We have also set $\Gamma_s = \rho_s(\Gamma)$. Let $H_s \subset \Gamma_s$ be the group generated by $h_{+,s}$ and $h_{-,s}$. We say that a *compressing pair* for ρ_s is a pair of subsets (U_1, U_2), having the following properties: First, $d(U_1) = U_2$. Second, there is a proper subset $V \subset U_1$ such that $h(U_2) \subset V$ for all $h \in H_s$.

Lemma 4.1 *If ρ_s has a compressing pair then ρ is a discrete embedding.*

Proof: Any element $g \in \Gamma$ has the property that

$$\rho_s(g) = h_n \circ d \circ h_{n-1} \circ d \circ \ldots \circ h_1$$

where $h_j \in H_s$. The elements h_n and h_1 can be trivial, but all the other h_j are nontrivial. We perform induction on n. The inductive hypothesis is the following: For $j = 1, 2$,

1. if h_n is trivial, then $\rho(g)(U_j) \subset d(V) \subset U_2$;
2. if h_n is nontrivial, then $\rho(g)(U_j) \subset h_n(U_2) \subset V$.

When $n = 1$, there is nothing to prove.

Suppose the induction hypothesis holds for $n-1$. If $h_n = 1$, then

$$\rho(g)U_j = \rho(d)\rho(h_{n-1} \circ d \ldots d \circ h_1)U_j \subset d(V)$$

If $h_n \neq 1$, then

$$\rho(g)U_j = \rho(h_n)\rho(d \circ h_{n-1} \circ d \ldots d \circ h_1)U_j \subset \rho(h_n)U_2 \subset V$$

as desired.

As in the Ping Pong lemma, we have shown that $\rho_s(g)$ does something uniformly nontrivial when g is not the identity element. Hence, ρ_s is a discrete embedding. ♠

4.2 The Projection

Recall that T is the Clifford torus. $S^3 - T$ consists of two open solid tori:

$$U_1 = \{(z,w)|\ |z| < |w|\} \cap S^3; \quad U_2 = \{(z,w)|\ |z| > |w|\} \cap S^3.$$

We will reprove the discreteness result in [**GP**] by showing that (U_1, U_2) is a compressing pair for ρ_s as long as $s \in [0, \underline{s}]$. In this section we reduce this to a problem about disks in the hyperbolic plane.

The condition $d(U_1) = U_2$ is true since $d(z,w) = (w,z)$. Let $W \subset \boldsymbol{CH}^2$ be the closed disk $\{z = 0\} \cap (\boldsymbol{CH}^2 \cup S^3)$. Let $\Pi_W : S^3 \to W$ be the projection $\Pi_W(z,w) = (0,w)$. For $j = 1, 2$, let $W_j = \Pi_W(U_j)$. By definition, W_2 is the open disk of (Euclidean) radius $\sqrt{2}/2$ centered at $(0,0)$, and W_1 is the annular region $\{(0,w)|\ |w| \in (\sqrt{2}/2, 1]\}$.

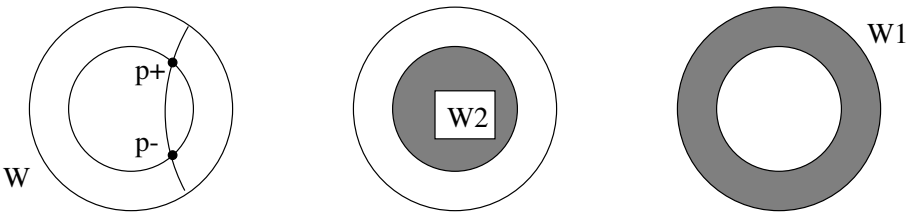

Figure 4.2.

Lemma 4.2 *(U_1, U_2) is a compressing pair for ρ_s if and only if $h(W_2) \subset W_1$. for all $h \in H_s$.*

Proof: Using the formula for h_+ given in §2.3 we see that $h_\pm \circ \Pi_W = \Pi_W \circ h_\pm$. Hence,

$$h \circ \Pi_W = \Pi_W \circ h; \qquad h \in H_s. \tag{32}$$

From this we see that $h(U_2) \subset U_1$ iff $h(W_2) \subset W_1$. If $h(W_2) \not\subset W_1$ then (U_1, U_2) is certainly not a compressing pair.

Suppose $h(W_2) \subset W_1$ for all $h \in H$. Note that $h(W_2)$ is a disk and W_1 is an annulus. Hence, every finite union of the form $\bigcup_{h \in H'} h(W_2)$ is a proper subset of W_1. Here H' is a finite subset of H. The element $h_\pm|_W$ is an isometric rotation about a point $p_\pm \in W$, as shown in Figure 4.2. Hence, the product $h_+ h_-$ is loxodromic, regardless of parameter.

The Euclidean diameter of the set $h(U_1)$ tends to 0 as the word length of h tends to ∞. This fact, together with the finite union property, implies that $X = \bigcup_{h \in H} h(W_2)$ is a proper subset of W_1. Thus, $V = \Pi_W^{-1}(X)$ is a proper subset of U_1 such that $h(U_2) \subset V$ for all $h \in H$. ♠

4.3 Patterns of Disks

The disks $\overline{W}_2$ and $h_\pm(\overline{W}_2)$ are tangent at the point $p_\pm$. Thus, the disks $hh_\pm(\overline{W}_2)$ and $h(\overline{W}_2)$ are tangent at the point $h(p_\pm)$. The points of tangency all lie on the geodesic A, through the points $p_\pm$. This geodesic is the translation axis for h_+h_-. Figure 4.3 shows two pictures of the situation. In the second half of Figure 4.3, the complex slice W has been identified with the upper half plane model and the geodesic A has been identified with the positive imaginary axis.

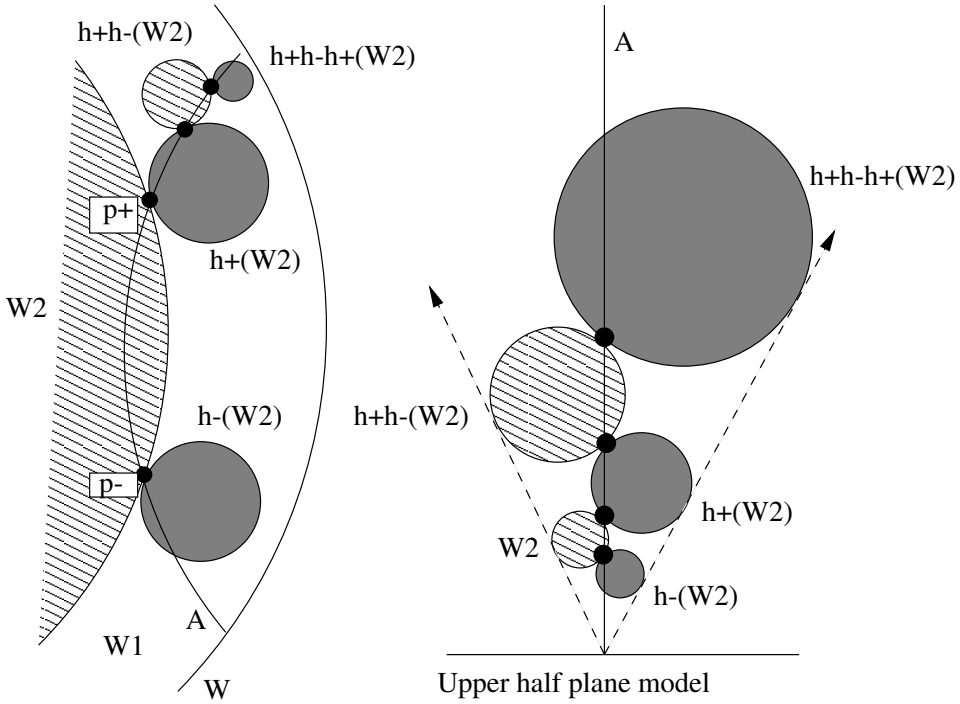

Figure 4.3.

If h has odd word length then h is an isometric rotation about a point not in W_2. Hence, $h(W_2) \subset W_1$ for words of odd length. If $h(W_2) \cap W_2 = \emptyset$ for some $h \in H$ having length $2k$ then $h'(W_2) \cap W_2 = \emptyset$ for all words h' having longer even length. The point is that the hyperbolic distance from the hyperbolic center of W_2 to the hyperbolic center of $h'(W_2)$ exceeds the hyperbolic distance from the hyperbolic center of W_2 to the hyperbolic center of $h(W_2)$. Our conclusion: If $h(W_2) \cap W_2 = \emptyset$, for h having word length 2, then (U_1, U_2) is a compressing pair at the parameter in question.

By symmetry $h_{+,s}h_{-,s}(W_2) \cap W_2 = \emptyset$ if and only if $h_{-,s}h_{+,s}(W_2) \cap W_2 = \emptyset$. A calculation, which we omit, shows that the distance between the hyperbolic center of W_2 and the hyperbolic center of $h_{+,2}h_{-,s}(W_2)$ is monotone decreasing in s, and that the two disks are tangent when $s = \underline{s}$. This establishes the discreteness result in [**GP**].

Remark: Our discreteness criterion parallels [**GP**, Lemma 3.2]. Our Lemma 4.2 parallels [**GP**, Lemma 3.3]. Our analysis in this section parallels the auxilliary Lemma used to prove [**GP**, Lemma 3.3]. Our omitted calculation parallels the calculation in [**GP**] which concludes their discreteness proof. Our Clifford torus is contained in the ideal boundary of the Dirichlet polyhedron considered in [**GP**]. Our map Π_W corresponds to the map Π_C used in [**GP**].

4.4 Another Point of View

The reader may think, at this point, that our proof above fails by accident. Let us give another point of view which shows that the proof must fail for structural reasons.

The fixed point $p_{\overline{s}}$ of $g_{\overline{s}}$ is contained in the Clifford torus, by symmetry. The point here is that the element r preserves the Clifford torus and conjugates $g_{\overline{s}}$ to its inverse. Let Q be the complex line tangent to S^3 at $p_{\overline{s}}$. The element $g_{\overline{s}}$ stabilizes Q, and rotates this plane nontrivially. Q is transverse to the Clifford torus T. This means that $g_{\overline{s}}(T)$ must intersect T transversely. For s sufficiently close to $\overline{s}$ the same phenomenon must occur, by continuity. One may think of $\underline{s}$ as the cutoff for this phenomenon. When $s \in (\underline{s}, \overline{s}]$, the element g_s does not have the translational strength to compensate for its rotational component in a direction transverse to T. In short, g_s does not have the strength to pull T off of itself.

5 The Hybrid Cone

5.1 The Basic Construction

Suppose that (E, p) is a pair, where E is a $\boldsymbol{C}$-circle and $p \in E$ is a point.

Lemma 5.1 *Suppose $x \in S^3 - E$. There is a unique $\boldsymbol{R}$-circle $\gamma = \gamma(E, p; x)$ such that $x \in \gamma$ and $p \in \gamma$ and $\gamma \cap (E - p) \neq \emptyset$.*

Proof: We normalize by a Heisenberg stereographic projection so that $E = E_0$, the center of $\mathcal{H}$, and $p = \infty$. In this case, there is a unique level Heisenberg $\boldsymbol{R}$-circle containing x. This is $\gamma(E_0, \infty; x)$. ♠

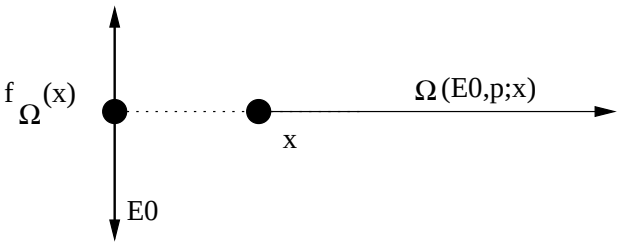

Figure 5.1.

Let $\Omega(E, p; x)$ be the arc of $\gamma(E, p; x)$ which connects X to p and which is disjoint from $E - p$. If $S \subset S^3 - E$ we define

$$\Omega(E, p; S) = \bigcup_{x \in S} \Omega(E, p; x). \tag{33}$$

We call $\Omega(E, p; S)$ the *hybrid cone* of S with respect to (E, p). We call the individual $\boldsymbol{R}$-arcs in the union above the *foliating arcs*.

Our construction is natural: $\Omega(T(E), T(p); T(S)) = T(\Omega(E, p; S))$, when T is the restriction to S^3 of an isometry of $\boldsymbol{CH}^2$.

We define the *endpoint map*

$$f_\Omega(x) = \gamma(E, p; x) \cap (E - p). \tag{34}$$

Remark: When $f_\Omega(S)$ is a single point, Ω is a subset of a *spinal sphere*. (See [**G**, Ch. 5] for the theory of spinal spheres.) Thus the hybrid cone construction generalizes the spinal sphere construction.

5.2 Hybrid Disks and Hybrid Sectors

Let (E, p) be as above. If S is a $\boldsymbol{C}$-arc, let $\widetilde{S}$ be the $\boldsymbol{C}$-circle which contains S. A *hybrid disk* is a hybrid cone of the form $\Omega(E, p; \widetilde{S})$. A *hybrid sector* is a hybrid cone of the form $\Omega(E, p; S)$, where S is a proper nontrivial $\boldsymbol{C}$-arc. We will sometimes write $\Omega(E, p; \widetilde{S}) = \widetilde{\Omega}(E, p; S)$

Lemma 5.2 *Let $\Omega = \Omega(E, p; S)$ be a hybrid sector. $\Omega - \partial\Omega$ is an analytically embedded open solid triangle. $\widetilde{\Omega} - p - C$ is an analytically embedded punctured open disk.*

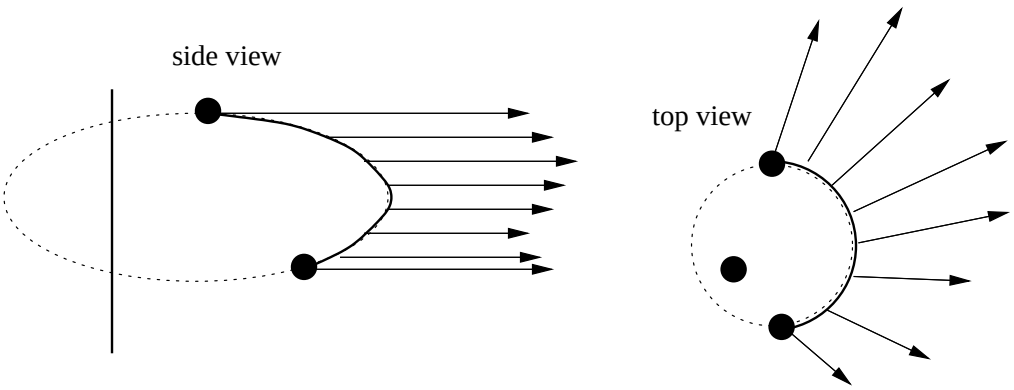

Figure 5.2.

Proof: We will consider the case of hybrid sectors, the case of hybrid disks being similar. We normalize by a Heisenberg stereographic projection so that $E = E_0$, the center of $\mathcal{H}$, and $p = \infty$. In this setting $\Omega(E_0, \infty; S) - \infty$ is a surface with boundary, ruled by rays. The ruling rays are arcs of level Heisenberg $\boldsymbol{R}$-circles. The endpoints of the rays are contained in S. The linking condition implies that the rays are pairwise disjoint. The rays certainly vary analytically with points on S. Our lemma is clear from this description. ♠

When $\Omega(E, p; S)$ is normalized as in the previous lemma, we say that it is in *standard position*. Figure 5.2 shows a picture of a standard position hybrid sector. The point ∞ is not shown. If continued in the other direction, all the foliating arcs of a standard position hybrid sector intersect the center E_0. This accounts for the radiating appearance of the top view.

5.3 Canonical Parametrization

In this section we describe a parametrization for hybrid sectors. The formulas for the parametrization are only important for the proof in the sense that our code actually uses these them.

Let $(E, p; S)$ be as above. Let q be the point of E diametrically opposed from p. (This makes sense because E is a round circle.) Let $\zeta \in S^3$ be some auxilliary point chosen so that p, q, ζ lie on a common $\boldsymbol{R}$-circle. Let $\{\hat{p}, \hat{q}, \hat{\zeta}\}$ be an equalized choice of lifts. Let E^* be the polar vector to E_s, chosen so that $\langle \zeta, E^* \rangle = \langle \hat{p}, \hat{q} \rangle$.

Let S be a $\boldsymbol{C}$-arc as above. Let S_1 and S_2 be the endpoints of S, and let S_3 be the midpoint of $\tilde{S} - S$. Referring to Equation 10 we define

$$S_t = C_{S_3}(S_1, S_2; t); \quad \hat{S}_t = \frac{\Theta^{-1}(S_t)}{\langle \Theta^{-1}(S_t), \hat{p} \rangle} \qquad t \in [0,1]. \tag{35}$$

$\hat{S}_t$ is the lift of S_t such that $\langle \hat{S}_t, \hat{p} \rangle = 1$. Now define

$$\hat{A}_t = \Im(\langle \hat{q}, \hat{S}_t \rangle)\ \hat{p} + i\hat{q} \qquad A_t = \Theta(\hat{A}_t). \tag{36}$$

Note that A_t lies on the complex slice determined by p and q. It is easily checked that $\langle \hat{A}_t, \hat{A}_t \rangle = 0$ and $\boldsymbol{A}(p, S_t, A_t) = 0$, so that $A_t = f_\Omega(S_t)$. Referring to Equation 13 the following map is a parametrization of $\Omega(E, p; S)$.

$$\Omega(E, p; S; t, u) = R_{A_t}(p, S_t; u); \quad (t, u) \in [0,1]^2. \tag{37}$$

5.4 The Elevation Map: Basics

We use the notation above. As above, the formulas in this section are only relevant to the proof in that we actually use them in our code.

Recall that $\pi(z, w) = (z, \Im(w))$. Define

$$Y_\zeta = \pi \circ \Theta \circ \hat{Y}_\zeta; \quad \hat{Y}_\zeta(x) = (\langle \tilde{x}, E^* \rangle, \langle \tilde{x}, \hat{q} \rangle, \langle \tilde{x}, \hat{p} \rangle) \tag{38}$$

It is easy to see that the vector $V(z, w) = w\hat{p} + \hat{q} + wE^*$ is null iff $\Re(w) = |z|^2$. Evidently $\Theta \circ \hat{Y}(V(z, w)) = (z, w)$. Thus $\Theta \circ \hat{Y} \circ \Theta^{-1}$ maps $S^3 - p$ into the boundary of the Siegel domain. In short, Y_ζ is a Heisenberg stereographic projection mapping $\Omega(E, p; S)$ to standard position, normalized so that $Y_\zeta(p) = \infty$ and $Y_\zeta(q) = (0, 0)$ and $Y_\zeta(\zeta) = (1, 0)$.

Let S^1 be the unit circle in $\boldsymbol{C}$. Let $\Upsilon = S^1 \times \boldsymbol{R}$. We define

$$\xi(z,t) = (z/|z|, t); \quad \pi_{\boldsymbol{R}}(z,t) = t \tag{39}$$

We define the ζ-*elevation map* $\Psi : S^3 - \{p\} \to \Upsilon$ as follows:

$$\Psi(x) = \begin{cases} \xi \circ Y_\zeta(x) & \text{if } x \in S^3 - E \\ \\ S^1 \times \pi_{\boldsymbol{R}} \circ Y_\zeta(x) & \text{if } x \in E - p \end{cases}$$

Technically, Ψ is a map from $S^3 - p$ to subsets of Υ. This detail is absorbed into the statements of our estimates.

Lemma 5.3 $\Psi(\Omega(E,p;S) - \{p\}) = \Psi(S)$.

Proof: Let $x \in S$ be a point. By construction, $Y(\Omega(E,p;x))$ is a ray of a level $\boldsymbol{R}$-circle. Thus, ξ is constant on $Y(\Omega(E,p;x))$. ♠

Say that a *barrier* for (E,p) is a pair (f,Ψ), where $f : S^1 \to \boldsymbol{R}$ is a continuous function. Let Λ_f be the graph of f in Υ. Let $\Lambda_{1,f}$ and $\Lambda_{2,f}$ be the two components of $\Upsilon - \Lambda_f$. We will take $\Lambda_{2,f}$ to be the component above Λ_f, as shown in Figure 5.3. In this figure, $S^1 \times \boldsymbol{R}$ is mapped into the plane via the map $(z,t) \to (\arg z, t)$.

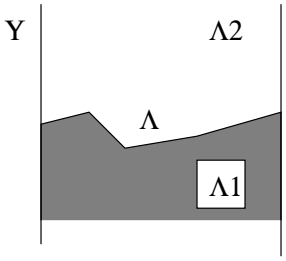

Figure 5.3.

Lemma 5.3 immediately implies

Lemma 5.4 *Let $\Omega = \Omega(E,p;S)$ be a hybrid sector. Suppose that $\gamma \in PU(2,1)$ stabilizes (E,p). Suppose $\Psi(\Omega) \subset \Lambda_{1,f}$ and $\Psi(\gamma(\Omega)) \subset \Lambda_{2,f}$. Then $\Omega \cap \gamma(\Omega) = \{p\}$.*

Remark: At this point, the reader interested in the parabolic case of the Main Theorem can skip to the next chapter.

5.5 The Elevation Map: Fine Points

Lemma 5.5 *Suppose that α is an $\boldsymbol{R}$-arc, contained in an $\boldsymbol{R}$-circle $\hat{\alpha}$. If $\hat{\alpha}$ intersects E in two points, neither of which is p, and α intersects E in one point, then $\pi_{\boldsymbol{R}} \circ \Psi$ is monotone on α.*

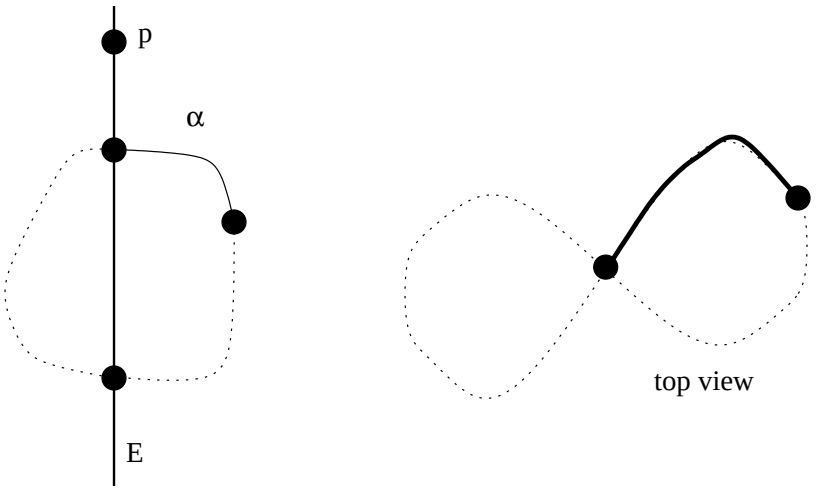

Figure 5.4.

Proof: We set $Y = Y_\zeta$, and recall that $\Psi = \xi \circ Y$, as above. $\pi_{\boldsymbol{C}} \circ Y(\hat{\alpha})$ is a lemniscate centered at the origin. $Y(\hat{\alpha})$ is a $\mathcal{E}$-integral lift of this lemniscate. The slope of this lift is only 0 at the two points which cover 0. In particular, the slope of $Y(\alpha)$ vanishes only at the endpoint. (See [**G**, p.141] for an explicit parametrization.) Hence, the height function is monotone on $Y(\alpha)$. ♠

Corollary 5.6 *Let $\Omega(E, p; S)$ be a hybrid disk. Suppose $\gamma \in PU(2,1)$ is such that $\gamma(E) = E$ but $\gamma(p) \neq p$. Suppose that $\Psi \circ \gamma(\partial\Omega) \subset \Lambda_2$ and $\pi_{\boldsymbol{R}} \circ \Psi \circ \gamma(p) > \max f$. Then $\Psi(\alpha) \subset \Lambda_{2,f}$ for some foliating arc α of $\gamma(\Omega)$.*

Proof: The curve $\Psi \circ \gamma(\partial\Omega)$ is a simple closed curve on Υ which, by hypothesis, is contained in $\Lambda_{2,f}$. This curve is a generator for the homology of Υ. From this it follows that there is some $x \in \gamma(\partial\Omega)$ such that $\pi_{\boldsymbol{R}} \circ \Psi(x) > \max f$. Let α be tha $\boldsymbol{R}$-arc of $\gamma(\Omega)$ which connects x to p. By Lemma 5.5, we have $\pi_{\boldsymbol{R}} \circ \Psi(y) > \max f$ for all $y \in \alpha$. This obviously implies that $\Psi(\alpha) \in \Lambda_{2,f}$. ♠

5.6 Tame Hybrid Disks

Say that a hybrid disk $\Omega(E, p; \widetilde{S})$ is *tame* if the surface $\Omega - \partial\Omega - p$ is never tangent to the distribution $\mathcal{E}$.

Lemma 5.7 *Let $\Omega(E, p; \widetilde{S})$ be a hybrid disk. Let E^* and S^* be polar vectors to E and $\widetilde{S}$. If $\hat{\delta}(E^*, S^*) < 1/4$ then $\Omega(E, p; \widetilde{S})$ is tame.*

Proof: Modulo $PU(2,1)$-equivalence, there is a one parameter family of inequivalent hybrid disks. To get a complete family, we normalize so that

$$E^* = (0, 1, 0); \quad S^* = (1/a, 1, 1); \quad p = (-1, 0).$$

Here $a \in [0, 1)$. We compute $\hat{\delta}(E^*, S^*) = a^2$. The map $\boldsymbol{B}_0$, defined in Equation 7, maps Ω to standard position. The points

$$p_1 = (0, 1); \quad p_2 = \left(\frac{2a}{1+a^2}, \frac{a^2-1}{1+a^2}\right)$$

belong to S. By symmetry, $\boldsymbol{B}_0(S)$ intersects $\boldsymbol{R} \times \{0\}$ at $\boldsymbol{B}_0(p_1) = (1, 0)$ and $\boldsymbol{B}_0(p_2) = (a-1, 0)$ and has center of mass $c = (a, 0)$. The point on $\pi_{\boldsymbol{C}} \circ \boldsymbol{B}_0(\Omega)$ having minimum norm is $\pi_{\boldsymbol{C}} \circ \boldsymbol{B}_0(p_2) = a - 1$. If $a \in [0, 1/2)$ then every point of $\pi_{\boldsymbol{C}} \circ \boldsymbol{B}_0(\Omega)$ has norm greater than a.

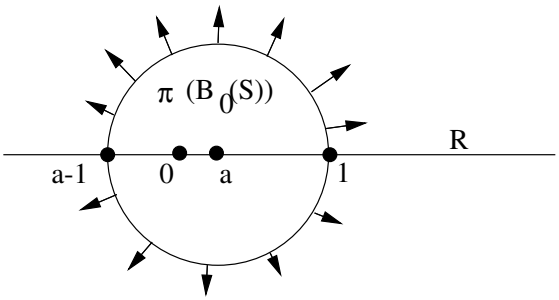

Figure 5.7.

Let T_x and E_x be the tangent plane and $\mathcal{E}$-plane at $x \in \boldsymbol{B}_0(\Omega - \widetilde{S}) - \infty$. Given any plane $\Pi \in \mathcal{H}$, we define the *slope* $s(\Pi) = \sup_{v \in \Pi} \pi_{\boldsymbol{R}}(v)/|\pi_{\boldsymbol{C}}(v)|$. From Equation 8 we have $s(E_x) = 2|\pi_1(x)| > 2|a|$. Now, $\boldsymbol{B}_0(\Omega)$ is ruled by horizontal rays, which have endpoints on Σ, and which lie on lines which intersect $\{0\} \times \boldsymbol{R}$. This geometry implies that $s(T_x) \leq s(E_c) = 2|a| < s(E_x)$. Hence, $S_x \neq E_x$. ♠

5.7 A Disjointness Criterion

Lemma 5.8 *Suppose that $I \subset \boldsymbol{R}^n$ is some connected open set. Suppose, for $t \in I$, that $\Omega(E, p_t; C_t)$ is a smoothly varying family of tame hybrid disks and $\Omega(E, q_t, S_t)$ is a smoothly varying family of hybrid sectors or hybrid disks. Suppose that*

1. *For each $t \in I$, we have $p_t \neq q_t$.*
2. *$C_t \cap \Omega(E, q_t; S_t) = \emptyset$ for all $t \in I$.*
3. *$S_t \cap \Omega(E, p_t; C_t) = \emptyset$ for all $t \in I$.*
4. *For some parameter $s \in I$, one of the foliating arcs of $\Omega(E, q_s, S_s)$ is disjoint from $\Omega(E, p_s, C_s)$.*

Then $\Omega(E, p_t, C_t) \cap \Omega(E, q_t, S_t) = \emptyset$ for all $t \in I$.

Proof: Let N denote the union of all foliating arcs of $\Omega(E, q_t, S_t)$. The parameter t ranges throughout I in this definition. We equip N with the Hausdorff topology: Two elements of N are close if they are contained in small tubular neighborhoods of each other. Obviously, N is connected.

Let $N' \subset N$ denote those arcs β such that β is a foliating arc for $\Omega(E, q_t; S_t)$ and β is disjoint from $\Omega(E, p_t; C_t)$. To establish this lemma, it suffices to prove that $N' = N$. Note that N' is nonempty, due to statement 4 above. N' is clearly open.

To finish the proof we show that N' is closed. Let $\beta_1, \beta_2...$ be a sequence of elements of N' which converge to some $\beta \in N$. Let t be the parameter associated to β.

1. Statement 1 above implies that $\beta \cap p_t = \emptyset$.
2. Statement 2 implies that $\beta \cap C_t = \emptyset$.
3. Statement 3 implies that $\partial\beta \cap \Omega(E, p_t, C_t) = \emptyset$.

The only possibility is that $\beta - \partial\beta$ intersects $\Omega(E, p_t, C_t) - C_t - p_t$. If this intersection is transverse, then nearby arcs, including some of the β_n, would intersect nearby hybrid disks. Hence $\beta - \partial\beta$ is tangent to $\Omega(E, p_t; C_t) - C_t - p_t$ at some point x.

There is a foliating arc of $\Omega(E, p_t, C_t)$ which contains x. Call it α. Since $\Omega(E, p_t, C_t)$ is tame, the plane E_x of $\mathcal{E}$ intersects the tangent plane T_x to $\Omega(E, p_t; C_t)$ transversely, in a line L. Both α and β are tangent to $\Omega(E, p_t, C_t)$ at x, and both α and β are $\mathcal{E}$-integral. Hence, α and β are both tangent to L. The important conclusion here is that α and β are therefore tangent to each other.

We normalize so that $\Omega(E, p_t; C_t)$ is in standard position. $\pi_{\boldsymbol{C}}(\alpha)$ is a straight line segment, contained on a ray through the origin. β is a Heisenberg $\boldsymbol{R}$-arc, contained in a Heisenberg $\boldsymbol{R}$-circle $\hat{\beta}$. The curve $\pi_{\boldsymbol{C}}(\alpha)$ and $\pi_{\boldsymbol{C}}(\beta)$ are tangent at $\pi_{\boldsymbol{C}}(x) \neq 0$.

There are two cases to consider. Suppose first that $\pi_{\boldsymbol{C}}(\beta)$ is a straight line. In this case, $\pi_{\boldsymbol{C}}(\hat{\alpha})$ and $\pi_{\boldsymbol{C}}(\hat{\beta})$ are the same line through the origin. This implies that $\hat{\alpha} = \hat{\beta}$. Hence $\partial\alpha \cap \beta \neq \emptyset$ or $\partial\alpha \cap \beta \neq \emptyset$. Either possibility contradicts our assumptions.

We conclude that $\pi_{\boldsymbol{C}}(\hat{\beta})$ is a lemniscate. Since $\hat{\beta}$ intersects E_0 twice, $\pi_{\boldsymbol{C}}(\hat{\beta})$ is a centered at the origin. However, a straight line ($\pi_{\boldsymbol{C}}(\hat{\alpha})$) through the origin cannot be tangent to a lemniscate centered at the origin ($\pi_{\boldsymbol{C}}(\hat{\beta})$) at a point ($\pi_{\boldsymbol{C}}(x)$) other than the origin. This is a contradiction. ♠

6 Dented Tori

6.1 Technical Calculation

Remark: For the reader only interested in the parabolic case, the first two sections of this chapter can be replaced by a single calculation at the parameter $\overline{s}$. One can just skim this material.

Recall that $E^*_s = (e(s), \overline{e}(s), 1)$ is the eigenvector to g_s, as in §3.4. Let S be the circle of radius $\sqrt{2}/2$. Let $p_1(s)$ and $q_1(s)$ be the points such that the tangent lines to S at $p_1(s)$ and $q_1(s)$ contain $e(s)$. That is:

$$p_1(e) = \frac{1 + i\sqrt{2|e|^2 - 1}}{2\overline{e}} \qquad p_2(e) = \frac{1 - i\sqrt{2|e|^2 - 1}}{2\overline{e}}. \tag{40}$$

Figure 5.1 shows a picture which is visually accurate for all $s \in J$.

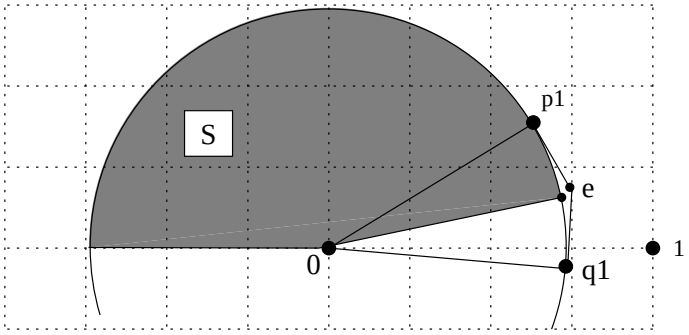

Figure 5.1

The following result implies that $p_1(s)$ never exits the shaded region of the picture and $q_1(s)$ never enters the shaded region.

Lemma 6.1 $\arg p_1(s) \in [\pi/12, \pi]$ *and* $\arg p_2(s) \in [\pi, 2\pi + \pi/12]$ *for all* $s \in J$.

Proof: Define $\theta_1 = \arg(e(\underline{s})) + 10^{-5}$ and $\theta_2 = \arg(e(\overline{s})) - 10^{-5}$. Also define $r_1 = |e(\underline{s})| + 10^{-5}$ and $r_2 = |e(\overline{s})| - 10^{-5}$. Finally, define $e_{ij} = r_i \exp(\theta_j)$. From the Near Monotonicity Lemma, and basic geometry, p_1 lies in the interval bounded by the outermost points $p_1(e_{ij})$ and q_1 lies in the interval bounded by the outermost points $q_1(e_{ij})$. Explicitly calculating, we obtain this lemma. Indeed, the points $p_1(e_{ij})$ and $q_1(e_{ij})$ are positioned almost exactly as those in Figure 5.1, independent of indices. ♠

6.2 The Axis Lemma

Define

$$\sigma = \tan(\pi/2 - \pi/12) = 2 + \sqrt{3}. \tag{41}$$

Let Δ_σ be the corresponding Clifford triangle, on the Clifford torus T. Let $\partial_h\Delta$ be the arc of the horizontal $\boldsymbol{C}$-circle which bounds Δ. Let $\partial_v\Delta$ be the arc of the vertical $\boldsymbol{C}$-circle which bounds Δ. Let $\partial_d\Delta$ be the arc of the diagonal $\boldsymbol{C}$-circle which bounds Δ. Thus, we have $\partial\Delta = \partial_h\Delta \cup \partial_v\Delta \cup \partial_d\Delta$.

Lemma 6.2 (Axis Lemma) *$E_s \cap T$ consists of two points. One of them, p_s, is contained in Δ_σ. The other point, q_s is not. Also E_s links each of the three $\boldsymbol{C}$-circles in $\partial\Delta_\sigma$.*

Proof: We repeat the notation from §6.1. Let S be the disk of radius $\sqrt{2}/2$ centered at the origin of $\boldsymbol{C}$. Let $p_1(s)$ and $q_1(s)$ be the two points of ∂S such that the tangent lines through these points contain $e(s)$. Define

$$p_s = (p_1(s), \overline{p}_1(s)); \quad q_s = (q_1(s), \overline{q}_1(s)). \tag{42}$$

We claim that $E_s \cap T = p_s \cup q_s$. By consruction, $p_s, q_s \in T$. Recall that $R = \{z = \overline{w}\} \cap S^3$. Note that $p_s, q_s \in R$. Since R is a round $\boldsymbol{R}$-circle, it is contained in the real slice $\hat{R} = \{z, \overline{z}\} \subset \boldsymbol{C}^2$. The map $\hat{R} \to \boldsymbol{C}$ given by $(z, \overline{z}) \to z$ carries R to the disk S and carries geodesics in $\hat{R}$ to straight lines in $\boldsymbol{C}$. Hence, the complex lines tangent to S^3 at p_s and q_s both contain E_s^*. This is enough to conclude that E_s^* is Hermitian perpendicular to p_s and q_s. Hence, $E_s \cap R = p_s \cup q_s$. If some other point o_s lies in $E_s \cap T$, then so does $r(o_s)$ which is contained in the same diagonal chain as o_s. This would force E_s to be a diagonal $\boldsymbol{C}$-circle, which it is not. The result of §6.1 is equivalent to the statement that $p_s \in \Delta$ and $q_s \notin \Delta$. for all $s \in J$.

Calculations show that

$$\hat{\delta}(E_{\overline{s}}^*, \partial_d\Delta^*) = .4; \quad \hat{\delta}(E_{\overline{s}}^*, \partial_h\Delta^*) = \hat{\delta}(E_{\overline{s}}^*, \partial_v\Delta^*) = .042938... \tag{43}$$

Here $\partial_d\Delta^*$ is a polar vector to the $\boldsymbol{C}$-circle containing $\partial_d\Delta$. Likewise for the other vectors.

Let x be any one of d, v, h. The calculation above shows that $E_{\overline{s}}$ links the $\boldsymbol{C}$-circle containing $\partial_x\Delta$. Since E_s never intersects the $\boldsymbol{C}$-circle containing $\partial_x\Delta$ for $s \in J$, we see that E_s always links this $\boldsymbol{C}$-circle. ♠

6.3 Main Construction

We define

$$\Omega_x(s) = \Omega(E_s, p_s; \partial_x \Delta); \qquad x = h, v, d. \tag{44}$$

For any subset $S \subset S^3$ let $dS = d(S)$. Here $d(z, w) = (w, z)$. Next, define

$$\Omega_\Delta(s) = \bigcup_{x=h,v,d} \Omega_x(s); \qquad \Omega(s) = \Omega_\Delta(s) \cup d\Omega_\Delta(s). \tag{45}$$

By construction, $\Omega(s)$ is the union of 6 hybrid sectors. Next, we define

$$\Xi = T - \Delta - d\Delta; \qquad \boldsymbol{Z}(s) = \Omega(s) \cup \Xi \tag{46}$$

We call $\boldsymbol{Z}(s)$ the *dented torus*. $\boldsymbol{Z}(s)$ has been constructed by cutting out two Clifford triangles from T and gluing back in 6 hybrid sectors. Figure 5.3 shows some of these sets schematically.

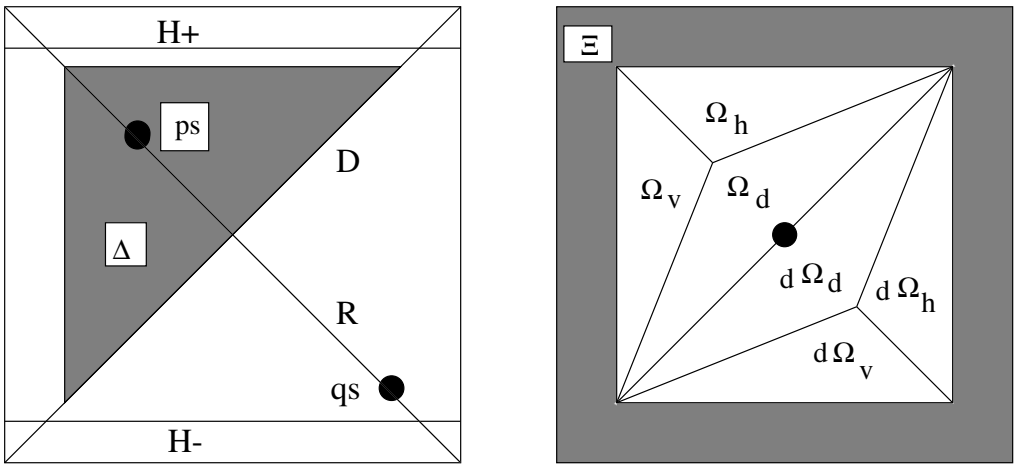

Figure 5.3

d preserves $\boldsymbol{Z}(s)$ by construction. r preserves Δ, $d\Delta$, Ξ, E_s, p_s, dE_s and dp_s, all the sets which are relevant to the construction. Thus $\boldsymbol{Z}(s)$ has 4-fold dihedral symmetry. In particular, the points p_s and q_s, which are fixed by r, are diametrically opposed on the circle E_s. Hence, the canonical parametrization of $\Omega_x(s)$, for $x = h, v, d$, uses the point q_s as the extra point.

Define

$$\zeta = \Big(-\frac{1}{\sqrt{2}}, -\frac{1}{\sqrt{2}} \Big). \tag{47}$$

Since $p_s, q_s, \zeta \in R$, the ζ-elevation map Ψ_s is well defined for the pair (E_s, p_s). By construction $\Psi_s(\Omega_x(s))$ is in standard position, for $x = h, v, d$.

7 The Discreteness Proof: Parabolic Case

7.1 Five Disks

Let W be the complex slice used in §4. Let W^* be the complex line $\{z = 0\}$ which contains W as its unit disk. Let $W^*_+ = \{(0, w) \in W^* | \ \Im(w) \geq 0\}$. Define W^*_- similarly. Let $A_{\overline{s}} \subset W$ be the translation axis of the element $h_{+,\overline{s}} h_{-,\overline{s}}$.

We define 5 disks which play a key role in our proof.

1. Let $W_A(\overline{s}) \subset W^*$ be the disk such that $A_{\overline{s}} \subset \partial W_A(\overline{s})$.
2. Let $W^+_B(\overline{s}) = h_{+,\overline{s}}(W_2)$.
3. Let $W^-_B(\overline{s}) = h_{-,\overline{s}}(W_2)$.
4. Let $W^+_C(\overline{s}) = h_{+,\overline{s}}(W_+*)$.
5. Let $W^-_C(\overline{s}) = h_{+,\overline{s}}(W_-*)$.

Let $W_{ABC}(\overline{s})$ be the union of these five disks. Here is a fairly accurate picture (Compare Figures 13.1-13.6.)

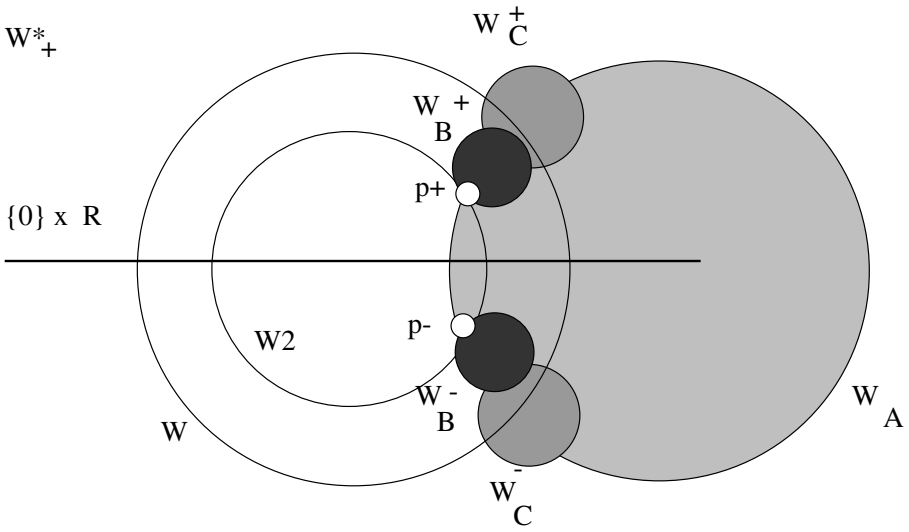

Figure 7.1

Henceforth we suppress the parameter $\overline{s}$.

Lemma 7.1 (Five Disk Lemma) *For all nontrivial $h \in H - H_2$ we have $h(W - W_{ABC}) \subset W_{ABC}$ and $h(W_2) \subset W_{ABC}$.*

Proof: We first deal with $W - W_{ABC}$. Suppose first h has odd length. By construction, h preserves the axis A, and interchanges the two components of $W - A$. Therefore,

$$h(W - W_{ABC}) \subset h(W - W_A) \subset W_A \subset W_{ABC} \tag{48}$$

By construction, $W - W_C^+ - W_C^-$ is a fundamental domain for the action of $h_+h_-h_+h_-$. Thus, if h has word length at least 4 we have

$$h(W - W_{ABC}) \subset h(W - W_C^+ - W_C^-) \subset W_C^+ \cup W_C^- \subset W_{ABC} \tag{49}$$

We now turn to the images of W_2. An explicit calculation shows that $W_2 \cap W_C^{\pm} = \emptyset$. Thus, $W_2 \subset W - W_C^{\pm} \subset W - W_{ABC}$. Equation 49 now implies that $h(W_2) \subset W_{ABC}$ when h has word length at least 4. If h has word length 1 then $h(W_2) \subset W_B$, by definition.

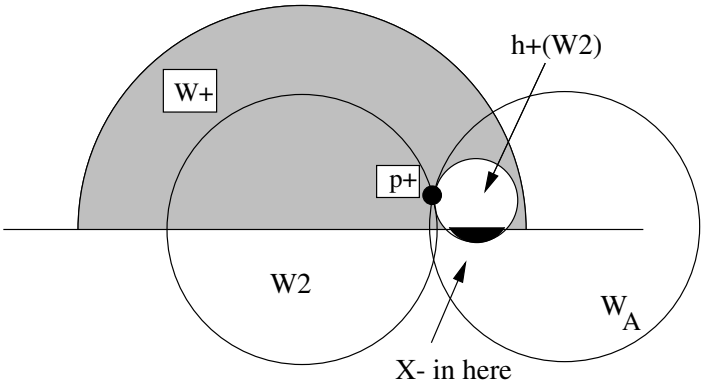

Figure 7.2

Suppose h has word length 3. By symmetry we can assume that $h = h_+h_-h_+$. Since $W_2 \cap W_B^{\pm} = \emptyset$ and $W_2 \cap W_C^{\pm} = \emptyset$, we have $W_2 - W_A \subset W - W_{ABC}$. Thus, we are reduced to showing that $h_+h_-h_+(W_2 \cap W_A) \subset W_{ABC}$. Let $X = h_+(W_2 \cap W_A)$. Let $X_{\pm} = X \cap W_{\pm}^*$. By construction, $h_+h_-(X_+) \subset W_C^+$. The region X_- if nonempty, is contained in W_A, by convexity, as shown in Figure 7.2. Thus,

$$h_+h_-(X_-) \subset h_+h_-(W_A) = W_A \subset W_{ABC}.$$

All in all, $h_+h_-h_+(W_2 \cap W_A) = h_+h_-(X) \subset W_{ABC}$, as desired. ♠

7.2 All Words but Two

Let $\boldsymbol{Z} = \boldsymbol{Z}(\overline{s})$ be the dented torus constructed in the previous chapter. Recall that $\boldsymbol{Z} = \Omega \cup \Xi$.

Lemma 7.2 (Estimate 1: Parabolic Case) $\Pi_W(\Omega_\Delta) \cap W_{ABC} = \emptyset$.

Proof: See §12. ♠

Corollary 7.3 $\Pi_W(\Omega) \cap W_{ABC} = \emptyset$.

Proof: Let r and d be as in Equation 18. This corollary follows from the fact that $\Omega = \Omega_\Delta \cup d\Omega_\Delta$, and rd commutes with Π_W, and $rd(W_{ABC}) = W_{ABC}$ and $rd(\Omega_\Delta) = d\Omega_\Delta$. ♠

Lemma 7.4 *If $h \in H - H_2$ is nontrivial then $h(\boldsymbol{Z}) \cap \boldsymbol{Z} = h(\Xi) \cap \Xi$.*

Proof: By the Five Disk Lemma, and Corollary 7.3, we have $h(\Pi_W(\Omega)) \subset W_{ABC}$. Hence $\Pi_W(\Omega) \cap \Pi_W(h(\Omega)) = \emptyset$. Pulling back, we have $\Omega \cap h(\Omega) = \emptyset$. By the Five Disk Lemma, we have $h(W_2) \subset W_{ABC}$. Hence, by Estimate 1, we have $\Pi_W(\Omega) \cap h(W_2) = \emptyset$. Pulling back by Π_W^{-1}, and using the fact that $\Pi_W(\Xi) \subset W_2$ we get $\Omega \cap h(\Xi) = \emptyset$. Since this is true for all nontrivial words $h \in H - H_2$ we have $\Omega \cap h^{-1}(\Xi) = \emptyset$. That is, $h(\Omega) \cap \Xi = \emptyset$. This result now follows from the fact that $\boldsymbol{Z} = \Omega \cup \Xi$. ♠

Let x be the attracting fixed point of h_+h_-. This point is one of the two intersection points of the axis A with ∂W. In particular,

$$x = \Pi_W(x) \subset W_A \subset W_{ABC}.$$

By Estimate 1, we have $x \notin \boldsymbol{Z}$. Let U_1 be the component of $S^3 - \boldsymbol{Z}$ which contains x.

Lemma 7.5 *If $y \in W_{ABC} - W_2$ then $\Pi_W^{-1}(y) \subset U_1$.*

Proof: Note that $W_{ABC} - W_2$ is path connected. Hence, there is a path $\delta_1 \subset W_{ABC} - W_2$ which joins y to x, the fixed point of h_+h_-. We can find a path $\delta_2 \subset S^3$ such that $\Pi_W(\delta_2) = \delta_1$. One endpoint of δ_2 is necessarily x, since $\Pi_W^{-1}(x) = \{x\}$. We can make the other endpoint any point of $\Pi_W^{-1}(y)$ we choose, since the fibers of Π_W are connected. By construction, $\delta_2 \subset S^3 - \boldsymbol{Z}$. ♠

Corollary 7.6 *Both fixed points of h_+h_- are contained in U_1. If σ is a fixed point of dh_+h_-d and $h \in H$ then $h(\sigma) \in U_1$.*

Proof: For the first claim, the fixed points of h_+h_- project to $\partial W \cap W_A \subset W_{ABC} - W_2$. For the second claim, the fixed points of h_+h_- have zero first coordinate. Hence, σ has zero second coordinate: $\Pi_W(\sigma) = (0,0) \notin W_A$. If h has odd length then $\Pi_W(h(\sigma)) = h(0,0) \subset W_A - W_2$. If h has even length, at least 4, then $\Pi_W(h(\sigma)) = h(0,0) \subset W_C^{\pm}$, which is disjoint from W_2. If h has length 2 then $h(0,0)$ is contained in $\partial W_C^{\pm}$. We have already seen that W_2 is disjoint from this disk. So, in all cases, $h(0,0) \in W_{ABC} - W_2$. Pulling back by Π_W, and applying Lemma 7.5 finishes the proof. ♠

Lemma 7.7 $U_1 \neq U_2$.

Proof: Let y be the fixed point of the parabolic element h_+d. Recall that H_+ is the horizontal chain on the Clifford torus which contains the horizontal arc bounding Δ, the Clifford triangle used in the construction of $\boldsymbol{Z}$. By construction $y \in H_+$. Hence, $\Pi_W(y)$ is the fixed point $p_+ \in W_2 \cap W_A$ of h_+. In particular, $\Pi_W(y) \subset W_{ABC}$.

Let x be the fixed point of h_+h_-. There is a path δ_0, connecting x to y, such that $\delta_0 - \{y\} \in U_1$, and δ_0 is transverse to Ξ at y. The path $\delta_1 = \delta_0 \cup d(\delta_0)$ joins $x \in U_1$ to $d(x) \in U_2$. By construction, δ_1 intersects Ξ transversely in a single point and is disjoint from $\boldsymbol{Z} - \Xi = \Omega$. If $U_1 = U_2$ then there is some path δ_1' which connects x to $d(x)$ but which avoids $\boldsymbol{Z}$. The path $\gamma = \delta_1 \cup \delta_1'$ is a closed loop in S^3 which intersects Ξ once, transversely, and is disjoint from Ω. Hence γ and $\partial\Omega = \partial\Xi$ are algebraically linked.

Homological considerations say that γ links $\partial\Delta$ or γ links $d\partial\Delta$, or both. Suppose, without loss of generality, that γ links $\partial\Delta$. Since Ω_Δ is the continuous image of a disk, attached to $\partial\Delta$ by a degree one map, we see that γ and Ω_Δ have nontrivial intersection. This is a contradiction. ♠

Lemma 7.8 *Let $h \in H - H_2$ be nontrivial. The component U_1 contains all but one component of $S^3 - h(\boldsymbol{Z})$.*

Proof: By Lemma 7.3 and Lemma 7.4 the intersection $X = h(\boldsymbol{Z}) \cap \boldsymbol{Z}$ is either the empty set, or one of the two $\boldsymbol{C}$-circles $H_\pm$. In either case, X does not disconnect $\boldsymbol{Z}$ and X does not disconnect $h(\boldsymbol{Z})$. Basic topology now implies that one component of $S^3 - \boldsymbol{Z}$, which we call the special component, contains all but one component of $S^3 - h(\boldsymbol{Z})$ (and *vice versa*.)

We now show that U_1 has nontrivial intersection with more than one component of $S^3 - h(\boldsymbol{Z})$, meaning that U_1 is the special component. Since h interchanges the fixed points of h_+h_-, both of which are contained in U_1, we see that $h(U_1) \cap U_1 \neq \emptyset$. From Corollary 7.6 we see that U_1 also contains $h(\sigma)$. Thus $h(U_2) \cap U_2 \neq \emptyset$. ♠

Lemma 7.9 *$h(U_2) \subset U_1$ for all nontrivial $h \in H - H_2$.*

Proof: We already know that U_1 contains all components of $S^3 - h(\boldsymbol{Z})$, except for one. We just have to rule out the possibility that $h(U_2)$ is this one exceptional component of $S^3 - h(\boldsymbol{Z})$. Assuming to the contrary, we get $h(U_1) \subset U_1$. The element rd conjugates h to h^{-1} and preserves $\boldsymbol{Z}$. Furthermore, since rd interchanges the fixed points of h_+h_-, we see that $rd(U_1) = U_1$. If $h(U_1) \subset U_1$ then

$$h^{-1}(U_1) = (rd)h(rd)(U_1) = (rd)h(U_1) \subset rd(U_1) = U_1.$$

This implies that $h^{-1}(U_1) \cap U_2 = \emptyset$. By Corollary 7.6 we have $h^{-1}(U_1) \cap U_2 \supset \{\sigma\} \neq \emptyset$, a contradiction. ♠

Remark: Computer evidence suggests that $\boldsymbol{Z}(\overline{s})$ is a tamely embedded topological torus and, in particular, that $S^3 - \boldsymbol{Z}(\overline{s})$ consists of exactly two connected components. If this was true, our argument above would somewhat simplify. While it is possible to convert the computer evidence into a proof, it is quite difficult to do so. We settle for slightly complicated arguments above to avoid the extremely complicated arguments needed to analyze the topology of $\boldsymbol{Z}(\overline{s})$.

7.3 Words of Length 2

Recall that $\Upsilon = S^1 \times \boldsymbol{R}^2$ and $\Psi : S^3 - p \to \Upsilon$ is the $\zeta = (1/\sqrt{2}, 1/\sqrt{2})$ elevation map associated to (E, p). Define

$$f(u) = t + .21\Im(\overline{z}u); \qquad (z^2, 2t) = \Psi \circ g(\zeta). \tag{50}$$

In defining z, the branch of $\sqrt{}$ is chosen so that $0 < \arg(z) < \arg(z^2)$. Let Λ and Λ_j be sets associated to the barrier (f, Ψ). We found this function experimentally.

Lemma 7.10 (Estimate 2: Parabolic Case) *For the parameter $\overline{s}$:*

1. $\Psi(\Xi \cup d\Omega_\Delta) \subset \Lambda_1(f)$.
2. $\Psi \circ g(d\Omega_\Delta \cup \Xi) \subset \Lambda_2(f)$.

Proof: See §12. ♠

Corollary 7.11 *$h(U_1) \subset U_1$ for $h \in H_2$.*

Proof: It suffices to consider the element h_+h_-, by symmetry. Note that $h_+h_-(\boldsymbol{Z}) = h_+h_-d(\boldsymbol{Z}) = g(\boldsymbol{Z})$. From Estimate 2 and Lemma 5.4 we have $g(\boldsymbol{Z}) \cap \boldsymbol{Z} = \{p\}$. Hence $h_+h_-(\boldsymbol{Z}) \cap \boldsymbol{Z} = \{p\}$. Since p disconnects neither $\boldsymbol{Z}$ nor $h_+h_-(\boldsymbol{Z})$, the same argument as above shows that $h_+h_-(U_2) \subset U_1$. ♠

All in all (U_1, U_2) is a compressing pair for ρ, and ρ is a discrete embedding.

8 The Year Lemma

We partition of J into 365 intervals of equal size. The set J_0 of midpoints of these intervals is the given by

$$(1 - \frac{2k-1}{730})\underline{s} + \frac{2k-1}{730}\overline{s}; \qquad k = 1, ..., 365. \tag{51}$$

Let I_k be the partition interval containing s_k

The geometry of $\boldsymbol{Z}(s)$ varies slowly with $s \in J$. However, this variation is extremely difficult to estimate directly. In this chapter we replace the family of sets $\{\boldsymbol{Z}(s)|\ s \in J\}$ by a family of sets $\{\boldsymbol{Z}(s_k, t)|\ t \in I_k;\ k = 1, ..., 365\}$. The set $\boldsymbol{Z}(s_k, t)$ is a replacement for $\boldsymbol{Z}(t)$, whose geometry is essentially the same as the geometry of $\boldsymbol{Z}(s_k)$. In this way, we only have to deal with the geometry of the surfaces $\boldsymbol{Z}(s_k)$, for $k = 1, ..., 365$.

8.1 Compatibility Maps

Let $s = s_k$, and $t \in I_k$ be some other parameter. Let (E_s, p_s) be the pair used to define $\boldsymbol{Z}(s)$. There are many maps $\phi_{st} \in PU(2,1)$ such that $\phi_{st}(E_s, p_s) = (E_t, p_t)$. In this section, we construct a canonical one which varies continuously with the parameters.

Let μ_s be the midpoint of the shorter of the two arcs of R which connects p_s to q_s. Likewise define μ_t. Let $r_s = \Theta(E_S^*) = (e(s), \overline{e}(s))$. Likewise define r_t. We define $\phi_{st} = \beta_{st} \circ \alpha_{st}$, where $\alpha_{st}, \beta_{st} \in PU(2,1)$ stabilize R and

1. α_{st} is a rotation such that $\alpha(\mu_s) = \mu_t$.

2. β_{st} is a pure translation along the line which joins $\alpha_{st}(r_s)$ to r_t.

By construction, ϕ_{st} commutes with the map r, which stabilizes R.

Let ρ be the round metric on S^3. For any map $\gamma \in PU(2,1)$, define $|\gamma| = \sup_{x \in S^3} \rho(x, \gamma(s))$. In particular, define $\epsilon_{st} = |\phi_{st}|$. As $t \to s$, we have $\epsilon_{st} \to 0$.

For any set $X \subset S^3$ let X^ϵ be the ϵ tubulr neighborhood of X, as measured in ρ. Define

$$B(s,t) = (\partial\Delta)^\epsilon; \qquad \epsilon = \epsilon_{st}. \tag{52}$$

$B(s,t)$ is a thin solid torus which surrounds $\partial\Delta$.

8.2 Main Construction

Define $\Omega(s,t) = \Omega_\Delta(s,t) \cup d\Omega_\Delta(s,t)$. Here

$$\Omega'_\Delta(s,t) = \phi_{st}(\Omega_\Delta(s)); \quad \Omega_\Delta(s,t) = \Omega'_\Delta(s,t) \cup B(s,t). \tag{53}$$

Finally, define

$$\boldsymbol{Z}(s,t) = \Xi \cup \Omega(s,t). \tag{54}$$

For later use, we define the elevation map

$$\Psi_{st} = \Psi_s \cup \phi_{st}^{-1}. \tag{55}$$

Here Ψ_s is the ζ-elevation map associated to the (E_s, p_s). By construction Ψ_{st} is the ζ'-elevation map for (E_t, p_t). Here $\zeta' = \phi_{st}(\zeta)$.

By construction,

$$\Omega'_\Delta(s,t) = \Omega(E_t, p_t; \phi_{st}\partial\Delta).$$

Thus, Ψ_{st} maps the hybrid sectors in $\Omega'_\Delta(s,t)$ to standard position. In particular, the hybrid sectors in $\Omega'_\Delta(s,t)$ are as well adapted to the element g_t as are the hybrid sectors in the discarded $\Omega_\Delta(t)$.

At the same time $\Omega'_\Delta(s,t)$ is a $PU(2,1)$-image of $\Omega_\Delta(s)$, and thus has essentially the same geometry. The object $\boldsymbol{Z}(s,t)$ retains the dihedral symmetry of $\boldsymbol{Z}(s)$. Finally, the set $B(s,t)$ seals up the gaps created by the discontinuous nature of our construction.

We will not actually deal with $\boldsymbol{Z}(s,t)$ directly. Rather, we will estimate the mismatch between $\boldsymbol{Z}(s,t)$ and $\boldsymbol{Z}(s)$.

Define $\Omega'_d(s,t) = \phi_{st}(\Omega_d(s))$. The remainder of the chapter is devoted to proving

Lemma 8.1 (Year Lemma) *Let $a = .00046$ and $b = .00221$. Let $s = s_k$ and $t \in I_k$.*

1. $\epsilon_{st} < a$.
2. $g_t(\Xi \cup d\Omega_\Delta(s,t)) \subset (g_s(\Xi \cup d\Omega(s))^b$.
3. $g_t(d\Omega'_d(s,t)) \subset (g_s(d\Omega_d(s)))^b$.

To avoid redundancy, we will just prove Statements 1 and 2. Statement 3 has the same proof as Statement 2.

8.3 Computational Ingredients

Lemma 8.2 *Let s_k be as above and let $t \in I_k$. There is a constant a_k such that*

1. $8||e(s_k)| - |e(t)|| + |\arg e(s_k) - \arg e(t)| < a_k < a$.
2. $4a_k + 2|s_j - t| < b$.

Proof: Let $\underline{s} = s_0, s_1, ..., s_{730} = \overline{s}$ be the set of 731 maximally and evenly spaced points in J_0. A straightforward calculation, detailed in §12, shows that, for successive values s_j, s_{j+1} we have

1. $8(||e(s_j)| - |e(s_{j+1})|| + 10^{-5}) + |\arg e(s_j) - \arg e(s_{j+1}) + 10^{-5}| = a_j < a$
2. $4a_j + 2|s_j - s_{j+1}| < b$

Each partition interval has the form $[s_{k-1}, s_{k+1}]$, with midpoint s_k. Here k is odd. The two items above, combined with the Near Monotonicity Lemma, give the result. ♠

Let $\Pi_Z : \boldsymbol{C}^2 \to \boldsymbol{C}$ be projection onto the first factor. Referring to Equation 23 define

$$\Sigma_k = \{x \in S^3 | \ \sup_{s \in J} |\Pi_Z(x) - P_0(s)| \geq 1/k\}. \quad P_0(s) = \frac{-\overline{A}_1(s)}{A_2(s)}. \tag{56}$$

The Lipshitz Lemma and the Variation Lemma below explain the significance of this set.

Lemma 8.3 (Part of Estimate 1) $(\Xi \cup d\Omega_\Delta(s))^b \subset \Sigma_3$ *for all* $s \in J_0$

Proof: See §9, Estimate 1. ♠

For later use, let $F_k \subset \Sigma_k \times \Sigma_k$ denote those points (x, y) which can be joined by a geodesic segment−i.e. an arc of a great circle−which is contained entirely in Σ_k.

8.4 Proof of Statement 1

Statement 1 of Lemma 8.2, together with the following Lemma, finishes the proof of Statement 1 of the Year Lemma.

Lemma 8.4 $\epsilon_{st} \leq |\arg(e(s)) - \arg(e(t))| + 8||e(s)| - |e(t)||$.

Proof: Recall that $\phi_{st} = \beta_{st} \circ \alpha_{st}$. Here α_{st} is a rotation which maps the midpoint μ_s to the midpoint μ_t. Now, μ_s is contained in the line through the origin which also contains the point $\Theta(E_s^*) = (e(s), \overline{e}(s))$. The corresponding statement holds for μ_t. From this it follows that

$$|\alpha_{st}| \leq |\arg(e(s)) - \arg(e(t))|.$$

It remains to show that $|\beta_{st}| \leq 8||e(s)| - |e(t)||$. From the Near Monotonicity Lemma, and from explicit evaluations at the endpoints of J,

$$\sup_{s \in J} \frac{\sqrt{2}}{2|e(s)|^2 - 1} < 8. \tag{57}$$

Let $\hat{R}$ be the real slice bounded by the round $\boldsymbol{R}$-circle R. Note that $\hat{R} = \{(z, \overline{z})\} \cap \boldsymbol{CH}^2$. We put the Euclidean metric on $\hat{R}$. By construction, the points

$$(0,0); \quad X_1 = \alpha_{st}(e(s), \overline{e}(s)); \quad X_2 = (e(t), \overline{e}(t))$$

are all contained in a single line L. The element β_{st} is a translation along L which maps $p_1 = \alpha_{st}(e(s), \overline{e}(s))$ to $p_2 = (e(t), \overline{e}(t))$. Note that

$$\|p_1\| = \sqrt{2}|e(s)|; \quad \|p_2\| = \sqrt{2}|e(t)|; \quad \|p_1 - p_2\| = \sqrt{2}||e(s)| - |e(t)||.$$

Combining this information with Lemma 2.3 and Equation 57 gives us our estimate on $|\beta_{st}|$. ♠

Corollary 8.5 *For any point $x \in \Xi \cup d\Omega_\Delta(s_k, t)$, there is some $y \in \Xi \cup d\Omega_\Delta(s_k)$ such that $\rho(x, y) < a_k$.*

Proof: Let $s = s_k$. Thie follows from the fact that ϕ_{st} moves every point of S^3 less than a_k. Hence, $d\Omega'_\Delta(s,t)$ is contained in the a_k-neighborhood of $d\Omega_\Delta(s)$. By construction, $B(s,t)$ is contained in the a-tubular neighborhood of $\Xi \cup d\Omega_\Delta(s)$. ♠

8.5 Proof of Statements 2

Lemma 8.6 (Lipschitz Estimate) *For all $(x,y) \in F_k$, and all $k \geq 0$,*

$$\sup_{(x,y)\in F_k} \frac{\rho(g_s(x), g_s(y))}{\rho(x,y)} \leq \frac{2k}{27}\sqrt{27+31k^2}.$$

In particular, the quantity on the right hand side is less than 4 for $k = 3$.

Proof: From the formula in §3.2 we have

$$g(z,w) = \left(\frac{w}{A_2 z + \overline{A_1}}, \frac{A_1 z - A_2}{A_2 z + \overline{A_1}}\right) = (g_1(z,w), g_2(z,w)).$$

Note that $|A_2(s)| \geq 3\sqrt{3}/2$ for $s \in J$. Let $P_0 = P_0(s)$ be as in Equation 56. We compute

$$|\partial_z g_1(s)| = \left|\frac{A_2 w}{(A_2 z - \overline{A}_1)^2}\right| \leq \frac{1}{|A_2||z-P_0|^2} \leq \frac{2k^2}{3\sqrt{3}}.$$

$$|\partial_z g_2(s)| = \left|\frac{A_2^2 - |A_1|^2}{(A_2 z - \overline{A}_1)^2}\right| \leq \frac{1}{|A_2|^2|z-P_0|^2} \leq \frac{4k^2}{27}.$$

$$|\partial_w (g_1)| = \left|\frac{1}{|A_2 z + \overline{A}_1|}\right| \leq \frac{1}{|A_2||z-P_0|} \leq \frac{2k}{3\sqrt{3}}.$$

$$\partial_w g_2 = 0.$$

The bound in this lemma follows from integrating the differential bound

$$\frac{\|dg(v)\|}{\|v\|} \leq \sqrt{|\partial_z g_1|^2 + |\partial_w g_1|^2 + |\partial_z g_2|^2 + |\partial_w g_2|^2}$$

along the arc of the great circle joining the two relevant points. ♠

Lemma 8.7 (Variation Estimate) *For all $s,t \in J$ and $x \in \Sigma_k$,*

$$\rho(g_s(x), g_t(s)) \leq \frac{2k}{3}|s-t|.$$

In particular, the quantity on the right hand side is less than $2|s-t|$ for $k = 3$.

Proof: Recall that

$$g = \Theta \circ \tilde{g} \circ \Theta^{-1}; \quad \Theta(z_1, z_2, z_3) = (z_1/z_3, z_2/z_3); \quad \Theta^{-1}(z, w) = (z, w, 1).$$

Let $X = (z, w) \in S^3$. Let $\tilde{X} = \Theta^{-1}(X) = (z, w, 1)$.

Inspecting the formula for $\tilde{g}$, we see that the third coordinate of $\tilde{g}(\tilde{X})$ has norm at least

$$|\overline{A}_1 + A_2 z| \geq |A_2|/k \geq \frac{3\sqrt{3}}{2k}.$$

Here we have used the same bound on $|A_2|$ as in the previous section. Let $N_0(\epsilon) \subset N_0$ denote those points (z_1, z_2, z_3) such that $|z_3| \geq \epsilon$. The above calculation shows that $\tilde{g}_s(\tilde{X}) \subset N_0(\frac{3\sqrt{3}}{2k})$. We compute the differential

$$d\Theta = \begin{bmatrix} 1/z_3 & 0 & -z_1/z_3^2 \\ 0 & 1/z_3 & -z_2/z_3^2 \end{bmatrix}.$$

Using the fact that $|z_1|^2 + |z_2|^2 = |z_3|^2$, we see that the sum of the squares of the matrix entries of $d\Theta$ is $3/|z_3|^2$. It follows that

$$\sup_{y \in N_0(\epsilon)} \frac{\|d\Theta(V)\|}{\|V\|} \leq \sqrt{3}\epsilon^{-1}.$$

Here V is any vector tangent to y.

Therefore, given $X \in \Sigma_k$, the path $g_s(X)$ has speed at most $\frac{2k}{3}$ times the speed of the path $\tilde{g}_s(\tilde{X})$, at corresponding points. An exercise in calculus shows that $|A_1'(s)| < .5$ and $|A_2'(s)| < .5$ for all $s \in J$. From this it follows that $\tilde{g}_s(\tilde{X})$ has speed at most 1. Hence, the path $g_s(X)$ has speed at most $\frac{2k}{3}$. This is a reformulation of this lemma. ♠

Let $x \in \Xi \cup d\Omega_\Delta(s,t))$ be arbitrary. By Corollary 8.5, there is some point $y \in \Xi \cup d\Omega_\Delta(s)$ such that $\rho(x, y) < a_k$. By Lemma 8.3, and the triangle inequality, the points x and y are both at least $b - a > a$ from $S^3 - \Sigma_3$. Hence, $(x, y) \in F_3$. From Lemmas 8.6 and 8.7

$$\frac{\rho(g_s(x), g_s(y))}{\rho(x, y)} \leq 4; \qquad g_s(x) - g_t(x) < 2|s - t|.$$

From the second statement of Lemma 8.2, and the triangle inequality:

$$\rho(g_t(x), g_s(y)) \leq \rho(g_t(x), g_s(x)) + \rho(g_s(x), g_s(y)) \leq 4a_j + 2|s - t| < b.$$

9 The Discreteness Proof: General Case

9.1 Five Disks

The set of disks $W_{ABC}(s)$ can be defined, for each parameter, just as in §7. Here we define a single collection W_{ABC}, which contains $W_{ABC}(s)$, for all $s \in J$. This collection is the union of the 5 disks defined below.

Lemma/Definition: *Let $W_A(s)$ be the disk in W such that $A_s \subset \partial W_A(s)$. Then $W_A(s) \subset W_A(s')$ if $s > s'$. In particular, we define $W_A = W_A(\underline{s})$, so that $W_A(s) \subset W_A$ for all $s \in J$*

Proof: Here A_s is the hyperbolic geodesic containing the fixed points of $h_{+,s}$ and $h_{-,s}$, which move together symmetrically along ∂W_2 as s increases. ♠

Lemma/Definition: *Let $W_B^{\pm}(s)$ be the disk tangent to W_2 at the fixed point $p_{\pm,s}$ of $h_{\pm,s}$, and also tangent to ∂W. Let $\sigma = (\underline{s} + \overline{s})/2$. Let W_B be the smallest disk, concentric with $W_B^{\pm}(\sigma)$ which contains both $W_B^{\pm}(\underline{s})$ and $W_B^{\pm}(\overline{s})$. Then $h_{\pm,s}(W_2) \subset W_B^{\pm}$ for all $s \in J$.*

Proof: By construction, $h_{\pm,s}(W_2) \subset W_B^{\pm}(s)$. Since the disk $W_B^{\pm}(s)$ are all isometric $W_B^{\pm}(s)$ are all Euclidean isometric to each other, and move monotonically through the annulus W_1, we see that $W_B^{\pm}(s) \subset W_B^{\pm}$ for all $s \in J$. ♠

Lemma/Definition: *Let $W_C^{\pm}(s) = h_{\pm,s}h_{\mp,s}(W_{\pm}^*)$. Then $W_C^{\pm}(s) \subset W_C^{\pm}(s')$ if $s < s'$. If we define $W_C^{\pm} = W_C^{\pm}(\overline{s})$ then $W_C^{\pm}(s) \subset W_C^{\pm}$ for all $s \in J$.*

Proof: We consider the case of W_C^+, the other case following from symmetry. $h_{+,s}h_{-,s}(\{0\} \times \boldsymbol{R}^2)$ is determined by its endpoints

$$h_+h_-(0,1) = \left(0, \frac{A_1 - A_2}{A_2 + \overline{A}_1}\right). \quad h_+h_-(0,-1) = \left(0, \frac{-A_1 - A_2}{A_2 - \overline{A}_1}\right).$$

These are the functions from Equation 23. An exercise in calculus show that the real parts (and hence the arguments) of the second coordinates of the above points are monotone for $s \in J$. Explicit evaluations at the endpoints of J show that $0 < \arg h_+h_-(0,1) < \arg h_+h_-(0,-1) < \pi/2$, that $\arg h_+h_-(0,1)$ decreases with the parameter and that $\arg h_+h_-(0,-1)$ increases. Hence $W_C^+(s) \subset W_C^+(\overline{s})$ for all $s \in J$. ♠

9.2 All Words but Two

Let a and b be as in the Year Lemma.

Lemma 9.1 (Estimate 1) *For all $s \in J_0$*

1. $\Pi_W((\Omega_\Delta(s))^a) \cap W_{ABC} = \emptyset$.
2. $(\Xi \cup d\Omega_\Delta(s))^b \subset \Sigma_3$, *the set from §8.*

Proof: See §12. ♠

Corollary 9.2 $\Pi_W(\Omega_\Delta(s,t)) \cap W_{ABC} = \emptyset$.

Proof: The same argument as in Corollary 8.5 implies that $\Omega_\Delta(s,t) \subset (\Omega_\Delta(s))^a$. The rest of the argument is immediate. ♠

The same symmetry as in §7 imples that $\Pi_W(\Omega(s,t)) \cap W_{ABC} = \emptyset$. As in §7, let $U_{1,t}$ be the component of $S^3 - \boldsymbol{Z}(s,t)$ which contains both fixed points of $h_{+,t}h_{-,t}$. Let $U_{2,t} = d(U_{1,t})$. Once we establish the following Lemma, the arguments in §7 apply *verbatim* to prove that $h(U_{2,t}) \subset U_{1,t}$ for all $h \in H_t - H_{2,t}$. The reader should bear in mind, while reading our proof, that the thin set $B(s,t)$ plays an important topological role in our proof.

Lemma 9.3 $U_{1,t} \neq U_{2,t}$.

Proof: Assume this result is false. Let x be as Lemma 7.7. The same argument in Lemma 7.7, combined with Lemma 9.2, implies that there is a loop $\gamma \in S^3 - \Omega(s,t)$ which links either $\partial\Delta$ or $d\partial\Delta$, or both. Assume, without loss of generality, that it is the former. $B(s,t)$ is a thin solid torus containing $\partial\Delta$ as its core curve. By construction, $\eta = \partial\Omega'_\Delta(s,t) \subset B(s,t)$. This latter curve runs nearly parallel to $\partial\Delta$, and is much longer than the cross sectional diameter of $B(s,t)$. Hence, η is nontrivial in the first homology of $B(s,t)$. In particular, γ and η are linked. The same argument as in Lemma 7.7 implies that γ intersects $\Omega'_\Delta(s,t)$, which is a contradiction. ♠

9.3 Words of Length 2

We found the following barrier function $f_s : S^1 \to \boldsymbol{R}$ experimentally:

$$f_s(u) = t(s) + (.21 + .11(s - \overline{s}))\ \Im(\overline{z}(s)u); \quad (z^2(s), 2t(s)) = \Psi_s \circ g_s(\zeta). \tag{58}$$

Here ζ is as in §7. We choose the branch of $\sqrt{\ }$ so that $z(s)$ varies continuously.

Let $\Lambda(s)$ and $\Lambda_j(s)$ be the sets associated to the barrier (f_s, Ψ_s), as in §7. Let $I_1(s) = (-\infty, t(s)]$ and $I_2(s) = [t(s), \infty)$.

Lemma 9.4 (Estimate 2) *Let $c = a + b$. For all $s \in J_0$ and for all $t \in I_s$,*

1. $\Psi_s(\Xi^c \cup (d\Omega_\Delta(s)^c) \subset \Lambda_1(s)$.
2. $\pi_{\boldsymbol{R}} \circ \Psi_s((d\Omega_d(s))^c) \subset I_1(s)$.
3. $\Psi_s(G_s) \subset \Lambda_2(s)$. *Here* $G_s = (g_s(\Xi))^c \cup (g_s(d\Omega_\Delta(s)))^c$.
4. $\pi_{\boldsymbol{R}} \circ \Psi_s(H_s) \subset I_2(s)$. *Here* $H_s = (g_s(d\Omega_d(s)))^c$.
5. $\pi_{\boldsymbol{R}} \circ \Psi_{st}(g_t(p_t)) > \max f_s$.
6. $g_t(p_t) \notin (\Xi \cup d\Omega_\Delta(s))^c$.

Proof: See §12. ♠

Corollary 9.5 *Let $s = s_k \in J_0$. For all $t \in I_k$, we have*

1. $\Psi_{st}(\Xi \cup d\Omega_\Delta(s,t)) \subset \Lambda_1(s)$.
2. $\pi_{\boldsymbol{R}} \circ \Psi_{st}(d\Omega_d(s,t)) \subset I_1(s)$.
3. $\Psi_{st} \circ g_t(\Xi \cup d\Omega(s,t)) \subset \Lambda_2(s)$.
4. $\pi_{\boldsymbol{R}} \circ \Psi_{st} \circ g_t(d\Omega_d(s,t)) \subset I_2(s)$.
5. $\pi_{\boldsymbol{R}} \circ \Psi_{st}(g_t(p_t)) > \max f_s$.
6. $g_t(p_t) \notin \Xi \cup d\Omega_\Delta(s,t)$.

Proof: Statement 1 of the Year Lemma, combined with the triangle inequality, say that

$$\phi_{st}^{-1}(\Xi \cup d\Omega_\Delta(s,t)) \subset (\Xi \cup d\Omega_\Delta(s))^{2a} \subset (\Xi \cup d\Omega_\Delta(s))^c.$$

We also know that $\Psi_{st} = \Psi_s \circ \phi_{st}^{-1}$. Hence, the set defined in the left hand side of Statement 1 of the Corollary is contained in the set defined in the left hand side of Statement 1 of Estimate 2. This proves Statement 1 of the Corollary. Statements 2-4 of the Corollary have very similar proofs. Statement 5 of the Corollary has just been copied down from Statement 5 of Estimate 2, for the sake of exposition. Statement 6 of the Corollary follows from Statement 6 of Estimate 2, and Statement 2 of the Year Lemma. ♠

Our goal is to show that $\boldsymbol{Z}(s,t) \cap g_t(\boldsymbol{Z}(s,t)) = \emptyset$ for $t \in I_k$. We also assume $t < \overline{s}$. Once this is done, the same argument as in §7 shows that $(U_{1,t}, U_{2,t})$ is a compressing pair for ρ_t.

Lemma 9.6 $\boldsymbol{Z}(s,t) \cap g_t(\boldsymbol{Z}(s,t) \subset \Omega'_\Delta(s,t) \cap g_t(\Omega'_\Delta(s,t))$.

Proof: By Lemma 5.3

$$\Psi_{st}(\Omega'_\Delta(s,t) - \{p_t\}) \subset \Psi_{st}(\partial\Omega'_\Delta(s,t)) = \Psi_s(\partial\Delta) \subset \Lambda_1(s).$$

Combining this with Statement 1 of Corollary 9.5, we have

$$\Psi_{st}(\boldsymbol{Z}(s,t) - \{p_t\})) \subset \Lambda_1(s).$$

Combining this with Statements 2 and 6 of Corollary 9.5 we have

$$\boldsymbol{Z}(s,t) \cap g_t(\Xi \cup d\Omega_\Delta(s,t)) = \emptyset.$$

The element r conjugates g_t to g_t^{-1} and preserves every relevant set. By symmetry, then,

$$g_t(\boldsymbol{Z}(s,t)) \cap (\Xi \cup d\Omega_\Delta(s,t)) = \emptyset.$$

This lemma now follows from the definition of $\boldsymbol{Z}(s,t)$. ♠

Lemma 9.7 $g_t(\Omega'_d(s,t)) \cap \Omega'_d(s,t) = \emptyset$.

Proof: First of all, we observe that $g_t(p_t) \neq p_t$, and $\Omega'_d(s,t)) \cap E_t = \{p_t\}$. $g_t(\Omega'_d(s,t)) \cap E_t = \{g_t(p_t)\}$. Hence,

$$p_t \notin g_t(\Omega'_d(s,t)) \cap \Omega'_d(s,t).$$

By Lemma 5.3 and Statement 2 of Corollary 9.5

$$\pi_{\boldsymbol{R}} \circ \Psi_{st}(\Omega'_d(s,t) - \{p_t\}) = \pi_{\boldsymbol{R}} \circ \Psi_{st}(\partial\Omega'_d(s,t)) \subset \pi_{\boldsymbol{R}} \circ \Psi_{st}(d\Omega_\Delta(s,t)) \subset I_1(s).$$

Similarly, by Statement 4 of Corollary 9.5,

$$\pi_{\boldsymbol{R}} \circ \Psi_{st} \circ g_t(\partial\Omega'_d(s,t)) \subset \pi_{\boldsymbol{R}} \circ \Psi_{st} \circ g_t(d\Omega_\Delta(s,t)) \subset I_2(s).$$

Applying Statement 5 of Corollary 9.5 and Lemma 3.4 to each of the foliating arcs of $g_t(\Omega'_d(s,t)$, we get

$$\pi_{\boldsymbol{R}} \circ \Psi_{st} \circ g_t(\Omega'_d(s,t)) \subset I_2(s).$$

Since $I_1(s) \cap I_2(s) = \emptyset$, the equations above combine to prove this lemma. ♠

Lemma 9.8 *Let $s \in J_0$, the set defined in §8. The hybrid disks $\widetilde{\Omega}_h(s)$ and $\widetilde{\Omega}_v(s)$ are tame.*

Proof: We check the hypothesis of Lemma 5.7 for each parameter in J_0. (Compare Equation 43.) See §12 for details of this calculation. ♠

Lemma 9.9 $\pi_{\boldsymbol{R}} \circ \Psi_s \circ g_s(\zeta) > \max f_s$, *for all $s \in J_0$.*

Proof: This is an explicit calculation. See §12 for details. ♠

Lemma 9.10 $g_t(\Omega'_d(s,t)) \cap \widetilde{\Omega}'_y(s,t) = \emptyset$ *for $y \in \{h, v\}$.*

Proof: We will take $y = h$. The case $y = v$ has the same proof. We will show that the tame hybrid disks $\widetilde{\Omega}_h(s,t)$ and the hybrid sectors $g_t(\Omega'_d(s,t))$ satisfy the hypotheses of Lemma 5.8.

1. The axis for $\widetilde{\Omega}'_h(s,t)$ is (E_t, p_t). The axis for $g_t(\Omega'_d(s,t))$ is $(E_t, g_t(p_t))$. Since $t \neq \overline{s}$, and since the fixed points of g_t are not contained in the Clifford torus, we have $q_t = g_t(p_t) \neq p_t$. This is hypothesis 1.

2. Since $\partial\widetilde{\Omega}'_d(s,t) \subset \Xi(s,t)$ and $\partial g_t\Omega_d(s,t) \subset g_t(\Xi(s,t))$, Lemma 9.6 implies that $\widetilde{\Omega}_d(s,t)$ and $g_t(\Omega_h(s,t))$ satisfy hypotheses 2 and 3.

3. Note that $g_s(\zeta) \subset g_s(\partial\Omega_d(s))$. Let α be the foliating arc of $g_s(d\Omega_d(s))$ which contains ζ. Lemma 9.9 implies that $\pi_{\boldsymbol{R}} \circ \Psi \circ g_s(\zeta) > \max f_s$. Statement 5 of Estimate 2 implies that $\pi_{\boldsymbol{R}} \circ \Psi \circ g_s(p_s) > \max f_s$. Lemma 5.5 now implies that $\Psi_s(\alpha) \subset \Lambda_2(s)$. From Lemma 5.3 and Estimate 2 we have $\Psi_s(\Omega(E_s, p_s; C_s) - \{p_s\}) \subset \Lambda_1(s)$. since $p_s \notin \alpha$, we see that $\alpha \cap \Omega(E_s, p_s; C_s) = \emptyset$. This is hypothesis 4.

♠

Lemma 9.11 *$g_t(\widetilde{\Omega}_x(s,t)) \cap \widetilde{\Omega}_y(s,t) = \emptyset$ for $x, y \in \{v, h\}$.*

Proof: The proof is the same as in the previous case. All we have to do is show that there is some foliating arc of $g_s(\widetilde{\Omega}_y(s,t))$ which is disjoint from $\widetilde{\Omega}_x(s,t)$. This follows from Estimate 2 and Corollary 5.6. ♠

10 Numerical Analysis

10.1 Clifford Torus Case

Recall that Ξ is the part of the dented torus which is also part of the Clifford torus. We subdivide Ξ into 5 Clifford rectangles, as shown in Figure 11.1. (What looks like 12 rectangles is really 5.) Let $\{\Xi_j : \ j = 1,2,3,4,5\}$ be the set of these pieces. Let $\Xi(t,u)$ be the rational parametrization of Ξ_j, as described in §2.7.

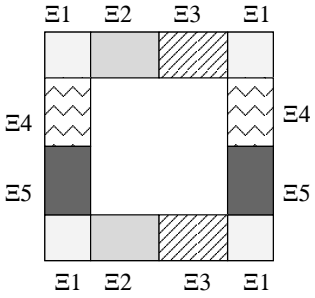

Figure 11.1

Given a rectangle $Q \subset [0,1]^2$, let $\Xi_j(Q)$ be Clifford subrectangle of Ξ_j parametrized by Q. We now construct a ball $B(\Xi_j, Q) \subset S^3$ such that $\Xi_j(Q) \subset B(\Xi_j, Q)$.

Let m be the midpoint of Q. Let V be the set of vertices of Q. Let $B(\Xi_j, Q)$ be the smallest ball centered at $\Xi_j(m)$ and containing the points $\Xi_j(V)$ in its boundary. All four points are contained in the boundary by symmetry. Since each $\boldsymbol{C}$-arc foliating Ξ_j is contained in a semicircle, we have $\Xi_j(Q) \subset B(\Xi_j, Q)$.

The *rectangle algorithm* computes $B(\Xi_j, Q)$, returns a 1 if the t-curves of $\Xi_j(Q)$ are longer than the u-curves and returns a 2 otherwise. The return of 1 tells the computer that it can more efficiently decrease the size of $\Xi_j(Q)$ by cutting Q in half so as to shorten the t-curves. A return of 2 tells the computer the opposite.

Remark: The analysis above uses, in a crucial way, the fact that the circular arcs in question are contained in semicircles. This property plays an important role in our analysis on several occasions. The key fact about such arcs is that their overall size is comparable to the distance between their endpoints. This is not true for circular arcs in general.

10.2 The Hybrid Sector Case

Given an arc $\gamma \subset S^3$, let $E(\gamma)$ denote the infimal $\epsilon > 0$ such that every point of γ is within ϵ of either endpoint of γ. For instance, if $\gamma = [0,1] \subset \boldsymbol{R}$ then $E(\gamma) = 1$.

Let $\Omega = \Omega(E, p; S)$ be a hybrid sector, with parametrization $\Omega(t,u)$. Let $T = [t_1, t_2]$ and $U = [u_1, u_2]$ be subintervals of $[0,1]$. Define

$$\Omega(T,u) = \bigcup_{t \in T} \Omega(t,u). \qquad \Omega(t,U) = \bigcup_{u \in U} \Omega(t,u). \tag{59}$$

$\Omega(t,U)$ is an $\boldsymbol{R}$-arc. We call $\Omega(T,u)$ a *transverse arc*. The goal of this chapter is to produce computable bounds $L_\Omega(t,U)$ and $W_\Omega(T,U)$ such that

1. $E(\Omega(t,U)) \le L_\Omega(t,U)$.
2. $E(\Omega(T,u)) \le W_\Omega(T,U)$ for any $u \in U$.

Our estimates are not general ones. We have only verified them for the *clean subsectors* of the hybrid sectors which actually participate in Estimates 1 and 2. (We will define below what we mean by *clean*.)

Let T_1 and T_2 be the two intervals obtained from splitting T in half. Likewise define U_1 and U_2. Let $m = (t_3, u_3)$ be the midpoint of Q. We have

$$\rho(\Omega(t,u), \Omega(m) \le \rho(\Omega(t,u), \Omega(t_3,u)) + \rho(\Omega(t_3,u), \Omega(t_3,u_3) \le$$

$$\max(W(T_1,U), W(T_2,U)) + \max(W(t_3,U_1), W(t_3,U_2)) = r(T,U).$$

Thus, $\Omega(Q)$ is contained in the ball $B(\Omega, Q)$ centered at $\Omega(m)$ and having radius $r(T,U)$.

The *rectangle algorithm* produces the ball $B(\Omega,Q)$. Also, it returns a 1 if $L_\Omega(t_1,U) \le W_\Omega(T,U)$, and returns a 2 if $L_\Omega(t_1,U) \ge W_\Omega(T,U)$. The integer values returned have a similar purpose as in the previous section.

10.3 Distortion of Stereographic Projection

Define

$$U(\epsilon) = \{(z,w) \in S^3 | \ |z+1| \le \epsilon\}. \tag{60}$$

Note that $U(2) = S^3$. Let $\boldsymbol{B}_0$ be the map from Equation 7. For any smooth map T, let dT be the linear differential of T.

Lemma 10.1 *If V is a unit tangent vector to S^3, based at a point $p \in U(\epsilon)$. Then $\|d\boldsymbol{B}_0(V)\| \geq 1/(\epsilon\sqrt{3})$. If V is $\mathcal{E}$-integral than $\|d(\pi_{\boldsymbol{C}} \circ \boldsymbol{B}_0)(V)| \geq 1/\epsilon$.*

Proof: By rotational symmetry, continuity, and integration, it suffices assume that $\boldsymbol{B}_0(p) \in \boldsymbol{R} \times \boldsymbol{R}$. Note that $\boldsymbol{B}_0^{-1}(\boldsymbol{R} \times \boldsymbol{R})$ consists of those points (z, w) such that $w/(z+1) \in \boldsymbol{R}$.

For $(z, w) \in \boldsymbol{B}_0^{-1}(\boldsymbol{R}^* \times \boldsymbol{R})$, define

$$\nu_r = \frac{(1+z)^2}{1+\overline{z}} \begin{bmatrix} -\overline{w} \\ \overline{z} \end{bmatrix}; \quad \nu_\theta = \begin{bmatrix} 0 \\ i(z+1) \end{bmatrix}; \quad \nu_t = \frac{1}{2} \begin{bmatrix} i(z+1)^2 \\ iw(z+1) \end{bmatrix}.$$

A vector ν is tangent to (resp. $\mathcal{E}$-integral) to S^3 at p if and only if $\Re\langle p, \nu\rangle = 0$ (resp $\langle p, \nu\rangle = 0$.) Using this criterion, we see that all three vectors above are tangent to S^3, and that ν_r is also $\mathcal{E}$-integral.

Observe that all vectors have norm at most ϵ. In the third case, this is a short exercise in calculus, which uses the fact that $|z|^2 + |w|^2 = 1$. We will show that $d\boldsymbol{B}_0$ maps the vectors above to an orthonormal basis. This implies our first differential bound. We will see, in particular, that $d(\pi_{\boldsymbol{C}} \circ \boldsymbol{B}_0)$ maps ν_r to a unit vector. This implies the second bound.

Let β_1 and β_2 be the component functions of $\boldsymbol{B}_0$. We compute

$$d\beta_1 = \Big(\frac{-w}{(1+z)^2}, \frac{1}{1+z}\Big).$$

$$d\beta_1(\nu_r) = 1; \quad d\beta_1(\nu_\theta) = i; \quad d\beta_1(\nu_t) = 0,$$

$$d\beta_2(\nu_t) = \pm \lim_{\epsilon \to 0} \frac{1}{\epsilon} \Im\Big[\frac{1-z}{1+z} - \frac{1-z-i\epsilon(z+1)^2/2}{1+z+i\epsilon(z+1)^2/2}\Big] = 1.$$

As we said above, ν_θ is a real multiple of $(0, iw)$, and this latter vector generates the flow $(z, w) \to (z, \exp(it)\ w)$. The map $\boldsymbol{B}_0$ conjugates this flow to the flow on $\mathcal{H}$ generated by $r\frac{d}{d\theta}$. Thus, we see that $d\beta_2(\nu_\theta) = 0$. The $\mathcal{E}$-integrality of $d\beta_1(\nu_r)$, together with the fact that $d\beta_1(\nu_r) = 1$, implies that $d\beta_2(\nu_r) = 0$. ♠

Lemma 10.2 *Suppose $(z, w) \in S^3 - U(\epsilon)$. If V is a unit tangent vector based at (z, w) then $\|d\boldsymbol{B}_0(V)\| \leq \sqrt{\epsilon^{-2} + 5\epsilon^{-4}} \leq \sqrt{6}\max(1, \epsilon^{-2})$.*

Proof: Let $\boldsymbol{B}_1$ be such that $\boldsymbol{B}_0 = \pi \circ \boldsymbol{B}_1$. Here $\pi(z,w) = (z, \Im(w))$. Note that $\|d\boldsymbol{B}_0(V)\| \leq \|d\boldsymbol{B}_1(V)\|$. We compute

$$d\boldsymbol{B}_1 = \begin{bmatrix} 1/(1+z) & w/(1+z)^2 \\ 2/(1+z)^2 & 0 \end{bmatrix}.$$

The lemma follows straightaway. ♠

10.4 Clean Hybrid Sectors

Let f_Ω be the endpoint map for $\Omega(E,p;S)$, as defined in §4.1. We say that $\Omega(E,p;S)$ is *clean* if

1. S is contained in a semicircle.
2. $f_\Omega(S) \subset E$ is contained in a semicircle.
3. f_Ω is injective on S.

Let Y be a Heisenberg stereographic projection mapping Ω to standard position. f_Ω is injective on S iff $\pi_{\boldsymbol{R}} \circ Y$ is injective on S. Now, $Y(S)$ is contained in an ellipse, so that $\pi_{\boldsymbol{R}}$ has at most one local maximum and one local minumum on $Y(S)$.

The *cleaning algorithm* does the following

1. Find the points $\{p_i\}$ of S where f_Ω is extremized.
2. Sort the points $\{m\} \cup \{p_i\}$, according to the order they appear on S. Here m is the midpoint of S.
3. Subdivide S into subarcs $\{S_i\}$, bounded by the sorted points.
4. Check that the hybrid sectors $\{\Omega(E,p;S_i\}$ are clean.

We implement the first step using a simple iterative method. We will explain how the method finds the point μ where $\pi_{\boldsymbol{R}} \circ Y$ attains its minimum. Finding the maximum point is similar. We first locate μ roughly, and thereby produce a map $\phi_0 : [0,1] \to \widetilde{S}$ whose image contains μ. Next, we evaluate the points $\pi_{\boldsymbol{R}} \circ Y \circ (\alpha(j/3))$ for $j = 0,1,2,3$. The minimum occurs either at $1/3$ or $2/3$. In the first case, we define $\phi_1 = \phi_0 \circ A_1$. Here A_1 is the affine map which takes $[0,1]$ to $[0,2/3]$. In the other case, we define $\phi_1 = \phi_0 \circ A_2$.

Here A_2 is the affine map which takes $[0,1]$ to $[1/3,1]$. Iterating, we get a sequence of maps $\phi_0, \phi_1, \phi_2...$ whose images rapidly converge to μ.

Let $\{S_i\}$ be the set of arcs produced by the first three steps of the cleaning algorithm. We will implement step 4 of the cleaning algorithm by showing p is further from either of the two points of $f_\Omega(\partial S_i)$ than these points are from each other.

10.5 Estimating the *R*-arcs

Let $\Omega(E,p;S)$ be a hybrid sector. Let S_t be the canonical parametrization for S. Let $A_t = f_\Omega(S_t)$ be the image of the endpoint map, as in §5.3. We define the *endpoint curves*:

$$E_p(t) = \boldsymbol{B}_0(-p \cdot A_t^{-1}); \qquad E_S(t) = \boldsymbol{B}_0(-S_t \cdot A_t^{-1}). \tag{61}$$

We have used the group law on S^3 to define these curves. More generally, we define

$$E\Omega(t,u) = -\Omega(t,u) \cdot A_t^{-1} \tag{62}$$

Lemma 10.3 $E\Omega(t,u) = uE_p(t) + (1-u)E_S(t)$

Proof: Apply Lemma 2.1 to the three points $X = -p \cdot A_t^{-1}$ and $Y = -S \cdot A_t^{-1}$ and $Z = -A_t \cdot A_t^{-1} = (-1,0)$. ♠

Combining Lemma 10.1 and Lemma 10.3 we see that, for all $u \in U$, we have $\rho(\Omega(t,u), \Omega(t,u_1) \le L_1(t,U)$, where

$$L_1(t,U) = [2]\ |u_1 - u_2|\ |\pi_{\boldsymbol{C}}(E_p(t)) - \pi_{\boldsymbol{C}}(E_S(t))|. \tag{63}$$

The 2 above is bracketed for purposes which will become clear in §10.7.

10.6 Estimating the Transverse Arcs

A *dyadic interval* is an interval of the form $[a/2^k, b/2^k]$, for a, b, k integers. When we run our main algorithm in the next section, we will only have to deal with dyadic subintervals of $[0,1]$. Our analysis of transverse arcs works for dyadic subintervals which have length at most $1/4$. If T is a longer interval, we set $W(T,U) = \pi$, the diameter of S^3. Henceforth, we assume that T is a dyadic subinterval of $[0,1]$, having length at most $1/4$.

We would like to compare $\omega_3 = \Omega(t_3, u)$ and $\omega_4 = \Omega(t_4, u)$, for $t_3, t_4 \in T$. The point ω_j lies in the $\boldsymbol{R}$-arc $\Omega_j = \Omega(t_j, [0,1])$. Let $A_j = A_{t_j}$ and $S_j = S_{t_j}$. Let R_j be right multiplication by $-A_j^{-1}$. Let $X_j' = R_j(X_j)$ for any point $X_j \in \Omega_j$. In particular, let $\Omega_j' = R_j(\Omega_j)$. We have $A_1' = A_2' = (-1, 0)$. Since R_j moves all points on S^3 the same distance, and since A_1, A_2, A_3, A_4 are contained, in order, on a semicircle, we get

$$\rho(\omega_3, \omega_4) < \rho(\omega_3', \omega_4') + \rho(A_3, A_4) \leq \rho(\omega_3', \omega_4') + \rho(A_1, A_2) \tag{64}$$

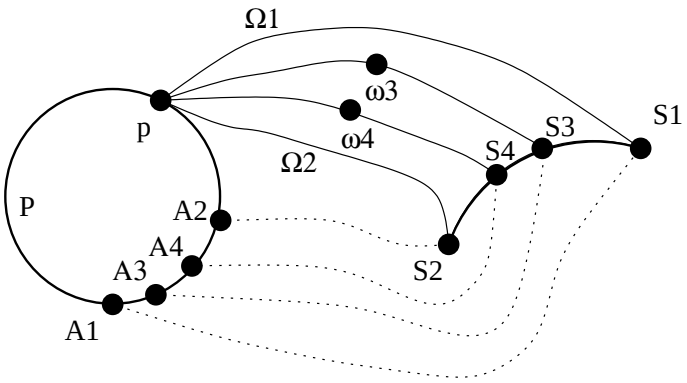

Figure 11.2.

Let $\boldsymbol{B}_0$ be the stereographic projection from Equation 7. Note that $\boldsymbol{B}_0(0, -1) = \infty$. Let $X'' = \boldsymbol{B}_0(X')$ for all relevant X. We equip $\mathcal{H}$ with the Euclidean norm. Below we prove

Lemma 10.4 *If Ω is a clean hybrid sector, produced when the cleaning algorithm is applied to a hybrid sector participating in Estimates 1 and 2, then*

$$\|p_3'' - p_4''\| \leq .002 + \|p_1'' - p_2''\| \qquad \|S_3'' - S_4''\| \leq .002 + \|S_1'' - S_2''\|$$

By Lemma 2.1, $\omega_j'' = up_j'' + (1-u)S_j''$. Combining this equation with Lemma 10.1, and Lemma 10.4, we see that $\rho(\omega_3', \omega_4') \leq W_1(T, u)$, where

$$W_1(T,u) = [2]\sqrt{3}\Big(.002 + u\|\boldsymbol{B}_0(R_1(p_1)) - \boldsymbol{B}_0(R_2(p_2))\| \\ +(1-u)\|\boldsymbol{B}_0(R_1(S_1)) - \boldsymbol{B}_0(R_2(S_2))\|\Big) \tag{65}$$

Again, 2 above is deliberately bracketed. The coefficients in the last equation are monotone for $u \in [0,1]$. Hence, independent of the choice of $u \in U$, we get $\rho(\omega_3', \omega_4') \leq W_1(T, U)$, where

$$W_1(T, U) = \max(W_1(T, u_1), W_1(T, u_2)) \tag{66}$$

10.7 Bootstrap Argument

Using the bounds above, we produce a ball $B'(\Omega, Q)$ such that $\Omega(Q) \subset B'(\Omega, Q)$. Our calculation of the radius of B' only depends on the fact that $\Omega(Q) \subset U(2)$. Given B', we find the best $\epsilon > 0$ such that $B' \subset U(\epsilon)$. Then, using the full force of Lemma 10.1, we can replace each occurence of the bracketed 2 above by ϵ. The smaller ball $B(\Omega, Q)$ also contains $\Omega(Q)$. Our bootstrap argument reduces our computation time roughly by a factor of 10.

10.8 Proof of Lemma 10.4

Let $\gamma : [0,1] \to \mathcal{H}$ is a curve. Given a dyadic subinterval $I \subset [0,1]$ let $B(\gamma, I)$ be the ball in $\mathcal{H}$ which has, as a diameter, the segment joining the two endpoints $\gamma(\partial I)$. Let I_m be the midpoint of I. Say that I is *good* if $\gamma(I_m) \subset B(\gamma, I)$.

Let $\mathcal{I}$ denote the set of dyadic subintervals of T. Say that a *Lipschitz estimator* for γ is map $\Lambda : \mathcal{I} \to \boldsymbol{R}$ such $\|\gamma(t) - \gamma(I_m)\| < \Lambda(I)$ for all $t \in I$. Consider this algorithm:

1. Let LIST be the partition of T consisting of just T.
2. If LIST is empty, halt. Otherwise...
3. let I be the first interval on LIST. If $\Lambda(I) \leq \epsilon$, delete I from LIST and go to Step 2. Otherwise... If I is good, replace I by the two intervals obtained by cutting I in half, and go to step 2. Otherwise fail.

If this algorithm halts without failure, the information constitutes a proof that $\gamma(t)$ is contained within the ϵ neighborhood of $B(\gamma, T)$. The point is that there is a sequence $T = T_0, T_1, ..., T_k$ of dyadic intervals such that $\|\gamma(t) - \gamma(\partial T_k)\| < \epsilon$ and $B(\gamma, T_k) \subset B(\gamma, T_{k-1}) ... \subset B(\gamma, T_0)$.

When run this algorithm, with the Lipschitz estimators defined below, for $\epsilon = .002$, and for the curves $p''(t) = \boldsymbol{B}_0(-p \cdot A_t^{-1})$ and $S''(t) = \boldsymbol{B}_0(-S_t \cdot A_t^{-1})$, it halts without failure for every parameter in $J_0 \cup \{\overline{s}\}$. See §12 for details of the calculation. This establishes the lemma.

Remark: For several parameters $s \in J_0$, one of the hybrid sectors produced by the cleaning algorithm is tiny. In these cases, checking the "control by balls" condition involves the comparison of two tiny quantities. The roundoff

error introduced by the computer interferes with this comparison. In these exceptional cases, we simply use our Lipschitz estimators to verify, in advance, that the relevant curves are entirely contained in a ball of radius .002, thereby bypassing our algorithm.

Lemma 10.5 *Let m be the midpoint of $[a, b]$. Let*

$$\lambda_1 = \max(\rho(A_a, A_m), \rho(A_b, A_m)); \quad \lambda_2 = |1 + \pi_1(-p \cdot A_m^{-1})| - \lambda_1$$

$\Lambda_p([a, b]) = \lambda_1\sqrt{6}\max(1, \lambda_2^{-2})$ *is a Lipschitz estimator for p''.*

Proof: Let m be the midpoint of $[a, b]$. Since $S|_T$ is contained in a semicircle, we have $\rho(p_c, p_m) \leq \lambda_1$. By the triangle inequality $\rho(p'_c, p'_m) \leq \lambda_1$. By definition, $p'_m = \boldsymbol{B}_0^{-1}(p''_m)$. Likewise for c. Therefore,

$$\rho(\boldsymbol{B}_0^{-1}(p''(c)), \boldsymbol{B}_0^{-1}(p''(m)) \leq \lambda_1.$$

By the triangle inequality,

$$|\pi_1(\boldsymbol{B}_0^{-1}(p''(t))) + 1| \geq \lambda_2; \quad t \in [c, m].$$

The points $\boldsymbol{B}_0^{-1}(p''(a))$ and $\boldsymbol{B}_0^{-1}(p''(c))$ can be connected by an arc having length at most λ_1. By Lemma 10.2, the restriction of $\boldsymbol{B}_0$ to this arc expands distances along this arc by at most $\sqrt{6}\max(1, \lambda_2^{-2})$. ♠

Essentially the same argument gives

Lemma 10.6 *Let m be the midpoint of $[a, b]$. Let*

$$\lambda_1 = \max(\rho(A_a, A_m), \rho(A_b, A_m)) + \max(\rho(S_a, S_m), \rho(S_b, S_m))$$

$$\lambda_2 = |1 + \pi_1(-S \cdot A_m^{-1})| - \lambda_1$$

$\Lambda_p([a, b]) = \lambda_1\sqrt{6}\max(1, \lambda_2^{-2})$ *is a Lipschitz estimator for S''.*

11 Verifying the Estimates

All our estimates work one parameter at a time. Suppose the parameter is fixed. The first step, in both cases, is to split the relevant hybrid sectors into clean hybrid sectors, and (for Estimate 2) to split Ξ into $\{\Xi_j\}$, as in §10.1.

Henceforth, we will say that a *piece* is either a clean hybrid sector participating in Estimates 1 and 2, or one of the Ξ_j. This chapter discusses how we verify that Estimates 1 and 2 hold for an individual piece. We will also explain the remaining statements in Estimate 2, which do not pertain to individual pieces.

11.1 Subdivision Algorithm

Let $Q_0 = [0,1]^2$. Given a *rectangle* $Q = [a_1, b_1] \times [a_2, b_2] \subset Q_0$, let

$$\Sigma_1(Q) = [a_1, (a_1+b_1)/2] \times [b_1, b_2] \cup [(a_1+b_1)/2, a_2] \times [b_1, b_2] \tag{67}$$

$$\Sigma_2(Q) = [a_1, a_2] \times [b_1, (b_1+b_2)/2] \cup [a_1, a_2] \times [(b_1+b_2)/, b_2] \tag{68}$$

These are the two dyadic subdivisions of Q into two rectangles. If $L = \{Q_k\}$ is a finite list of rectangles, let $\Sigma_j(L)$ be the list obtained from L by deleting the last rectangle Q_n and appending $\Sigma_j(Q_n)$.

Let $\mathcal{Q}$ denote the set of rectangles of $[0,1]^2$. Say that a *subdivision test* is a map $T : \mathcal{Q} \to \{0,1,2\}$. We are interested in proving the existence of a partition of Q_0 into rectangles $\{Q_1, ..., Q_n\}$ such $T(Q_j) = 0$ for $j = 1, ..., n$. Here is the *subdivision algorithm*:

1. Let LIST be a list with Q_0 as its only member.
2. If LIST is empty, halt. If not, let Q be the last rectangle in LIST.
3. If $T(Q) = 0$ delete Q from LIST and go to step 2.
4. If $T(Q) = j \in \{1,2\}$ then replace LIST by Σ_j(LIST) and go to step 2.

If the subdivision algorithm halts, the information constitutes a proof that the desired partition exists.

11.2 Estimate 1

Let a and b be as in Estimate 1. Let Ω be a piece. Let $Q \subset [0,1]^2$ be a rectangle. Let P_0 and Σ_k be as in Equation 56. Here is the subdivision test

1. Let $B = B(\Omega, Q)$ be the ball produced by the rectangle algorithm. Let (c, r) be the center and radius of B. Let $j \in \{1, 2\}$ be the integer produced by the rectangle algorithm.

2. For $i = 1, 2, 3, 4, 5$, let $\{(c_i, r_i)\}$ be the collections of centers and radii for the disks in W_{ABC}. If $\min_i(|\Pi_W(c) - c_i| - r - r_i) \leq a$, let $T(Q) = j$. Otherwise...

3. If $(\|\Pi_W \circ d(c)) - P_0(s)\| - \frac{1}{3} - r \leq b$, let $T(Q) = j$. Otherwise let $T(Q) = 0$.

$P_0(s)$ is evaluated from Equation 56. See §12.6 for a list of the centers and radii of the disks used in this estimate.

11.3 Variation of the Barrier Function

We use the notation of §9.3. Let f_s be the barrier function in Equation 58. Let $\pi_1 : S^1 \times \boldsymbol{R} \to S^1$ be projection. Let Ψ_s be the elevation map associated to the parameter s. For $q \in S^3$ define

$$F_s(q) = f_s \circ \pi_1 \circ \Psi_s(q) + \pi_{\boldsymbol{R}} \circ \Psi_s(q). \tag{69}$$

$$G_s(q) = \pi_{\boldsymbol{R}} \circ \Psi_s(q) - t(s) \tag{70}$$

We have defined this function so that

1. $\Psi_s(p) \in \Lambda_1(s)$ iff $F_s(p) < 0$

2. $\Psi_s(p) \in \Lambda_2(s)$ iff $F_s(p) > 0$.

3. $\pi_{\boldsymbol{R}} \circ \Psi_s(p) \in I_1$ iff $G_s(p) < 0$.

4. $\pi_{\boldsymbol{R}} \circ \Psi_s(p) \in I_2$ iff $G_s(p) > 0$.

Let $B \subset S^3$ be a ball with center c and radius r. We define $F_s(B) = \bigcup_{x \in B} F_s(b)$. If $p \in B$ we redefine $F_s(B) = [-10, 10]$, which causes B to fail all further tests applied to it. If $c = 0$, we replace B by the ball of radius $r + .0000001$ centered at $.0000001$. Henceforth, we assume that $c \neq 0$ and $p \notin B$. We also assume that the parameter s is fixed. Let $\tilde{c}$ be the affinely normalized lift of c.

Given a vector $V = (z_1, z_2, z_3)$, let

$$\|V\|_2 = \sqrt{|z_1|^2 + |z_2|^2}. \tag{71}$$

Define

$$L_+(B, V) = |\langle \tilde{c}, V \rangle| + r\|V\|_2; \qquad L_-(B, V) = \max(0, |\langle \tilde{c}, V \rangle| - r\|V\|_2). \tag{72}$$

Let $\hat{p}_s$ and $\hat{q}_s$ be any lifts of the points $p_s, q_s \in E_s$. Let $\hat{E}_s^*$ be any vector polar to E_s. Let r be the radius of B. Define

$$\alpha_1 = \min\Big(2\pi, \frac{r\|\hat{E}_s^*\|_2}{|L_-(B, \hat{E}_s^*)|} + \frac{r\|\hat{p}_s\|_2}{|L_-(B, \hat{p}_s)|}\Big). \tag{73}$$

$$\epsilon_1 = \min(\alpha_1, 2)\beta(s); \qquad \beta(s) = .21 + .11(s - \overline{s}) \tag{74}$$

$$\epsilon_2 = \frac{r\|\hat{q}_s\|_2}{L_-(B, p_s)} + \frac{r\|\hat{p}_s\|_2 L_+(B, \hat{q}_s)}{L_-(B, p_s)^2} \tag{75}$$

Lemma 11.1 (Barrier Test) *With the above notation*

1. *If* $F_s(c) + \epsilon_1 + \epsilon_2 < 0$ *then* $\Psi_s(B) \subset \Lambda_1$.
2. *If* $F_s(c) - \epsilon_1 - \epsilon_2 > 0$ *then* $\Psi(B) \subset \Lambda_2$.
3. *If* $G_s(c) + \epsilon_2 < 0$ *then* $\pi_{\boldsymbol{R}} \circ \Psi_s(B) \subset I_1$.
4. *If* $G_s(c) - \epsilon_2 > 0$ *then* $\pi_{\boldsymbol{R}} \circ \Psi_s(B) \subset I_2$.
5. *If* $G_s(c) + \epsilon_2 + \beta(s) < 0$ *then* $\Psi_s(B) \subset \Lambda_1$.
6. *If* $G_s(c) - \epsilon_2 - \beta(s) > 0$ *then* $\Psi_s(B) \subset \Lambda_2$.

Proof: Let $q \in B$ be an arbitrary point. We define $(z_q, t_q) = \Psi_s(q)$. Likewise $(z_c, t_c) = \Psi_s(c)$. We first prove that

$$A = |\arg(z_c) - \arg(z_q)| \leq \alpha_1. \tag{76}$$

To see this, let $\gamma : [0, \delta] \to S^3$ be a constant speed geodesic which connects c to p. Let $\tilde{\gamma}$ be the affinely normalized lift of γ. We certainly have $A \leq 2\pi$. Define $X(t) = \arg(\Psi \circ \gamma(t))$. By integration we have

$$A \leq \sup_t \|X'(t)\|\delta < \sup_t \|X'(t)\|r.$$

By definition we have

$$X(t) = \arg\left[\frac{\langle \tilde{\gamma}(t), \hat{E}_s^* \rangle}{\langle \tilde{\gamma}(t), \hat{p}_s \rangle}\right] = \Im L(t); \qquad L(t) = \log\left[\frac{\langle \tilde{\gamma}(t), \hat{E}_s^* \rangle}{\langle \tilde{\gamma}(t), \hat{p}_s \rangle}\right].$$

Here log is a branch of the complex logarithm. By calculus,

$$|X'(t)| \leq \|L'(t)\| = \left|\frac{\langle \tilde{\gamma}'(t), \hat{E}_s^* \rangle}{\langle \tilde{\gamma}(t), \hat{E}_s^* \rangle}\right| + \left|\frac{\langle \tilde{\gamma}'(t), \hat{p}_s \rangle}{\langle \tilde{\gamma}(t), \hat{p}_s \rangle}\right|.$$

The third coordinate of $\gamma'(t)$ is zero and $\|\gamma'(t)\| = 1$. By the Cauchy-Schwarz inequality,

$$|\langle \gamma'(t), V \rangle| \leq \|V\|_2.$$

Here V is any vector whose third coordinate is 0. Another application of the Cauchy-Schwarz inequality gives

$$|\langle \gamma(t), V \rangle| \geq L_-(B, V).$$

Therefore

$$|X'(t)| \leq \frac{\|\hat{E}^*\|_2}{L_-(B, \hat{E}^*)} + \frac{\|\hat{p}\|_2}{L_-(B, \hat{p})} = \epsilon_1.$$

Equation 76 follows straight from this.

A very similar argument proves

$$|t_q - t_c| \leq \epsilon_2. \tag{77}$$

Given the definition of f_s, we have

$$\max f_s - \min f_s = 2\beta(s); \qquad |df_s/du| \leq \beta(s). \tag{78}$$

The first inequality in Equation 78 immediately gives

$$f_s \circ \pi_1 \circ \Psi_s(c) - f_s \circ \pi_1 \circ \Psi_s(q) \leq 2\beta(s). \tag{79}$$

Integrating the second inequality in Equation 78 over the portion of S^1 which contains $\pi_1 \circ \Psi_s(B)$, we get

$$f_s \circ \pi_1 \circ \Psi_s(c) - f_s \circ \pi_1 \circ \Psi_s(q) \leq \alpha_1\beta(s). \tag{80}$$

Combining Equations 77, 79 and 80 we see that $|F_s(q) - F_s(c)| < \epsilon_1 + \epsilon_2$. Hence $F_s(q) < 0$. This is equivalent to the statement that $\Psi(q) \subset \Lambda_1$. The other statements have similar proofs. ♠

11.4 Acting on the Ball

Let Σ_k and $P_0(s)$, and F_k be as in Lemma 8.6. Let $B \in S^3$ be a ball, with radius r and center c.

Define

$$k = \frac{1}{|\pi_1(c) - P(s)| - r} \qquad K = \min(4, \frac{2k}{27}\sqrt{27 + 31k^2}). \tag{81}$$

Lemma 11.2 *$g_s(B) \subset X(B, g_s)$, where $X(B, g_s)$ is the ball having center $g_s(c)$ and radius Kr.*

Proof: By construction, every point $x \in B$ has the property that $(c, x) \in F_k$. Therefore, the Lipschitz constant of $g|_B$ is at most K by Lemma 8.6. ♠

11.5 Confining a Particular Curve

Let $s \in J_0$ and let I_s be the corresponding partition interval. Let p_s be the point used in the definition of the hybrid sectors of $\Omega_\Delta(s)$

Lemma 11.3 *Let β_s be the ball of radius .001 centered at $g_s(p_s)$. Then $(g_t(p_t))^a \in \beta_s$ for all $t \in I_s$.*

Proof: Recall that $a = .00046$. Let $P_0(s)$ be as in Equation 56 Define

$$k = \frac{1}{|\pi_1(p_s) - P_0(s)| - 2a - .02}; \quad K_1 = \frac{2k}{27}\sqrt{27 + 31k^2}; \quad K_2 = \frac{2k}{3}|I_s| \tag{82}$$

From the Year Lemma, $\rho(p_s, p_t) < a$. An exercise in calculus shows that the real and imaginary parts of $P_0(s)$ are monotone in s. Evaluating at the endpoints, we see that $|P_0(s) - P_0(t)| < .02$ for all $s, t \in J$. By the triangle inequality, $|\pi_1(p_t) - P_0(t)| < |\pi_1(p_s) - P_0(s)| + .02 + a$. We have chosen our constant k so that the geodesic in S^3 which joins p_s to p_t remains in Σ_k. Hence, $(p_s, p_t) \in F_t$. Applying Lemma 8.6 we see that $\rho(g_t(p_s), g_t(p_t)) < K_1 a$. Applying Lemma 8.7 we see that $\rho(g_s(p_s), g_t(p_s)) < K_2$. By the triangle inequality, $\rho(g_s(p_s), g_t(p_t)) \le K_1 a + K_2$. An explicit calculation, for all $s \in J$ shows that the right hand side of this equation is at most $.00054 = .001 - a$. See §12 for details. ♠

Corollary 11.4 *Statement 6 of Estimate 2 is true.*

Proof: Let $m_+(s)$ be the maximum value on S_1 attained by f_s. Let

$$x_s = Y_s^{-1}(0, m_+(s)).$$

Here Y_s is the Heisenberg stereographic projection used to define Ψ_s. Let $T_t = \pi_{\boldsymbol{R}} \circ \Psi_{st} \circ g_t$. We compute explicitly that $T_s(p_s) > \max f$ for all $s \in J_0$. (See §12 for details of the calculation.) We know that $g_t(p_t) \neq p_t$, and $T_t(p_t) = \infty$. Thus, $T_t(p_t) \neq \infty$. To verify Statement 6, we just have to rule out the possitility that $T_t(p_t) = m_+(s)$. If $T_t(p_t) = m_+(s)$ then $Y_{st} \circ g_t(p_t) = Y_s \circ \phi_{st}^{-1} \circ g_t(p_t) = Y_s(x_s) = (0, m_+(s))$. In other words, $\phi_{st}(x_s) = g_t(p_t)$. Hence, $x_s \in \beta_s$. For each parameter $s \in J_0$ we compute explicitly that $x_s \notin \beta_s$. See §12 for details. ♠

11.6 Estimate 2

Let Ω be a piece. Let $Q \subset [0,1]$ be a rectangle. Here is the subdivision test for Estimate 2.

1. Let $B = dB(\Omega, Q)$, where $B(\Omega, Q)$ is the ball returned from the rectangle algorithm. Let $j \in \{1, 2\}$ be the integer returned from the rectangle algorithm.

2. (Statement 1) Use the Barrier Tests to see if $\Psi(B^a) \subset \Lambda_1$. If not, set $T(Q) = j$. Otherwise...

3. (Statement 2, when relevant) Use the Barrier Tests to see if $\pi_{\boldsymbol{R}} \circ \Psi(B^a) \subset I_1$. If not, set $T(Q) = j$. Otherwise...

4. Let $B_g = X(g_s, B)$.

5. (Statement 3) Use the Barrier Tests to see if $\Psi(B_g) \subset \Lambda_2$. If not, let $T(Q) = j$. Otherwise...

6. (Statement 4, when relevant) Use the Barrier Tests to see if $\pi_{\boldsymbol{R}} \circ \Psi(B_g) \subset I_2$. If not, let $T(Q) = j$. Otherwise...

7. (Statement 5) If $B \cap \beta_s \neq \emptyset$ set $T(Q) = j$. Otherwise...

8. Set $T(Q) = 0$.

12 Implementation and Roundoff Error

12.1 Overview

The bulk of our computing is done in C. We use C code for Lemma 10.4 and also for Estimates 1 and 2. The C program only uses mathematical operations which are governed by the IEEE standards [**I**]. Namely

1. The $+, -, \times, \div$ and $\sqrt{}$ operations;
2. The $<$ and $>$ operations.
3. decimal $\Leftrightarrow$ binary conversion.

We implement our code using interval arithmetic, so that the computations themselves produce the error bounds.

There are a number of places in the paper where we need a small amount of fairly precise computation. We perform these computations in Mathematica [**W**], which has arbitrary precision arithmetic. We compute all quantities to roughly 20 decimal places of precision. While Mathematica is not guaranteed to be free from computational bugs (and bugs have been found!) we think there is general agreement that Mathematica does not have bugs in the basic operations we use−the ordinary arithmetic operations and the numerical extraction of cube roots. We have ruled out such computational bugs by random tests on our data−e.g. plugging the root of a cubic back into the cubic.

The C program relies on some initial values, depending on the parameter s. For instance, the C program needs to have the vector E_s^*. which in turn depends on the eigenvalues of g_s. Our Mathematica code computes all initial values for the C code, and stores them in auxilliary files. When the C code runs, it reads in these files as needed. Thus, the C code never has to compute any quantity which depends on functions which are not listed above.

We will first discuss certain features of our Mathematica code. Following this, we will explain explain how the computer represents real numbers, and how we implement interval arithmetic. At the end of this chapter, we give a record of all the calculations.

12.2 The Mathematica Code

Let g_s be the matrix in Equation 23. Let $E_s^* = (e(s), \overline{e}(s), 1)$ be the affinely normalized eigenvector associated to λ_s. Equation 30 gives $e(s)$ as a linear function of λ_s. Computing $e(s)$ accurately boils down to computing λ_s accurately. Once we have an accurate value of λ_s, all our Mathematica calculations are straightforward implementations of what is explained in the paper.

Finding the roots of the charactistic polynomial for g_s leads to the formula

$$\lambda_s = \frac{a(s) + b(s) + c(s)}{12(1+s^2)} \tag{83}$$

$$a(s) = -68 + 64is - 4s^2 \tag{84}$$

$$\begin{aligned} b(s) = 8\exp(4\pi i/3)(&-775 + 1734is + 1203s^2 - 308is^3 - 69s^4 \\ &+6is^5 + s^6 + 6\sqrt{3}(1+s^2)^{3/2}\sqrt{3s^3 - 125})^{1/3} \end{aligned} \tag{85}$$

$$c(s) = \frac{5440 - 7936is - 2688s^2 + 256is^3 + 64s^4}{b(s)} \tag{86}$$

This formula is valid, in particular, for $s \in J$. Once Mathematica chooses branches of the square and cube root functions, it can compute the expression above to, say, 1000 decimal places. We will stop at 20 decimal places.

Mathematica can consistently choose a branch of the square root function for all $s \in J$. Mathematica takes the positive branch of $\sqrt{1+s^2}$ and the positive imaginary branch of $\sqrt{3s^2 - 125}$. Mathematica needs to take a cube root in order to evaluate $b(s)$. We have Mathematica compute $b(s)$ along with λ_s. For successive computed parameters $s_1, s_2 \in J$, Mathematica checks

$$|b(s_j)| > 50; \qquad |b(s_1) - b(s_2)| < 1 \tag{87}$$

These bounds show that Mathematica cannot switch branches of the cube root when computing successive parameters. An explicit check shows that Mathematica chooses the correct branches for $\overline{s}$. Hence, the correct branches are always taken during the computation.

Once again, we ruled out computational bugs in the Mathematica code by randomly checking that the computed eigenvalues and eigenvectors are indeed eigenvalues and eigenvectors.

12.3 Performing the Cleaning Algorithm

For each of the 366 parameters $s \in J_0 \cup \{\overline{s}\}$, we perform the cleaning algorithm on the hybrid sectors in $\Omega_\Delta(s)$. Each of the resulting clean hybrid sectors $\Omega(E_s, p_s; S^j)$ is specified by the parameter s, the *axis*, which is the collection $\{E_s^*, \hat{p}_s, \hat{q}_s, \hat{\zeta}\}$ normalized as in §5.4, and an equalized choice of lifts $\{\hat{S}_1^j, \hat{S}_2^j, \hat{S}_3^j\}$. Here S_1^j and S_2^j are the endpoints of S^j and S_3^j is the midpoint of $\widetilde{S}^j - S^j$.

The axis is the same for all the hybrid sectors. The real and imaginary parts of the components of all relevant vectors are what is stored in the file. Everything is stored to 20 significant digits. (This is slightly more precision than is used in our C code.) The routine `Clean[datas,s]` performs the cleaning algorithm for the parameter s and stores the result in the file `data`s. The data contained in the created files is read in by the C code at the time of its operation.

12.4 Doubles

Our C code represents real numbers by *doubles*. According to [**I**,§3.2.2], a double $[x]$ is an object of the form (s, e, f). Here

1. s is a single bit, determining the sign of x.
2. e is an 11 bit word, representing an integer between 0 and 2047.
3. $f = \cdot b_1 ... b_{52}$ is 52 bit word.

The real number represented by $[x]$ is

$$r([x]) = (-1)^s \; 2^{e-1023}\Big(1 + \sum_{j=1}^{52} 2^{-j} b_j\Big). \tag{88}$$

(The exceptions to this formula, which are detailed in [**I**, §3.2.2], do not arise in our calculations.) For example, `3ff6a09e667f3bcd` represents the double closest to $\sqrt{2.0}$ The first bit of `3=0011` is `0`. Thus $s = 0$. The concatenation of `011` and `ff=11111111` is `01111111111`. Thus $e = 1023$, and $(-1)^s 2^{e-1023} = 1$. The word `6a...` expands as `01101010...`. Thus

$$\sqrt{2.0} = 1 + \quad 0 + \frac{1}{4} + \frac{1}{8} + 0 + \frac{1}{32} + 0 + \frac{1}{128} + 0... = 1.414...$$

To access the words comprising a double, we introduce an *exact*:

```
typedef struct
{int a,b;} exact;
```

Given an exact `E`, the integer `E.a` represents the first 32 bit word of the double (the *high bits*) and the integer `E.b` represents the second 32 bit word of the double (the *low bits*). Here is the code which enables one to convert between doubles and exacts.

```
exact double-to-exact(x)
double x;
{
exact E;
double *pointer1;
int *pointer2;
pointer1=&x;
pointer2=((int*) pointer1);
E.a=*pointer2;
++pointer2;
E.b=*pointer2;
return(E);
}

double exact-to-double(E)
exact E;
{
double x;
double *pointer1;
int *pointer2;
pointer1=&x;
pointer2=((int*) pointer1);
*pointer2=E.a;
++pointer2;
*pointer2=E.b;
return(x);
}
```

12.5 Interval Arithmetic

Let $\boldsymbol{D}$ be the set of doubles. Define $\boldsymbol{R}_0 = \{x \in \boldsymbol{R} |\ |x| < 2^{1023}\}$. Summarizing [**I**, §3.2.2, 4.1, 5.6], there is a map $\boldsymbol{R}_0 \to \boldsymbol{D}$, which maps each point $x \in \boldsymbol{R}_0$ to some $[x] \in \boldsymbol{D}$ which is closest to x. In case there are several equally close choices, the computer chooses one, as detailed in [**I**, §4.1].

Regarding the five basic operations, [**I**, §5] states that *each of the operations shall be performed as if it first produced an intermediate result correct to infinite precision and with unbounded range, and then coerced this intermediate result to fit into the destination's format.* Thus,

$$\sqrt{[x]} := [\sqrt{r([x])}] \qquad [x] * [y] := [r([x]) * r([y])] \quad * \in \{+, -, \times, \div\} \tag{89}$$

We order exacts lexicographically, simply by concatenating the two integers, treating it as a single integer. The inclusion $r : \boldsymbol{D} \to \boldsymbol{R}$ induces a linear order on the doubles. Beautifully, the linear order on positive doubles *coincides* with the linear order we have imposed on the corresponding exacts. Every double x (except the largest and smallest) has a unique successor $x_+ > x$ and a unique predecessor $x_- < x$. To compute these, we convert x to an exact, concatenate the integers, add 1 or -1, split apart the resulting integer, and convert back.

One exceptional case requires mention: To avoid a certain kind of underflow error, we redefined $0_\pm$ to be the double closest to $\pm 10^{-50}$. In hindsight, this redefinition seems unnecessary. At any rate, it is certainly harmless to our calculations.

An *interval* is a pair $I = (x, y)$ of doubles, such that $x \leq y$. Say that I *bounds* $z \in \boldsymbol{R}_0$ if $x \leq [z] \leq y$. This is true iff $x \leq z \leq y$. Define

$$[x, y]_o = [x_-, y_+] \tag{90}$$

Let $\partial_1 I$ and $\partial_2 I$ be the endpoints of an interval I. For $j = 1, 2$, let $I_j = ([x_j], [y_j])$ be intervals. For $* \in \{+, -, \times, \div\}$ we define

$$I_1 * I_2 = (\min_{i,j} \partial_i I_1 * \partial_j I_2,\ \max_{i,j} \partial_i I_1 * \partial_j I_2])_o; \qquad \sqrt{I} = (\sqrt{[x]}, \sqrt{[y]})_o \tag{91}$$

In all cases, one performs the relevant computations on the endpoints of the interval and then pushes the interval one click outward, to guarantee that

1. If I_j bounds x_j then $I_1 * I_2$ bounds $x_1 * x_2$.

2. If $I > 0$ bounds $x > 0$ then $\sqrt{I}$ bounds $\sqrt{x}$.

The only exception to this rule occurs when we are computing I_1/I_2, and the two endpoints of I_2 have different signs. In this case we automatically fail whatever computational test we are working on.

A potential problem, related to the exceptional case, is that we might divide by a very small number, producing an overflow error. All the tests performed by our code fail if a calculation produces a sufficiently large number. Thus, an overflow error does not occur in the calculations which are relevant to our proof.

We define a *complex interval* to be an expression of the form $X+iY$, where X and Y are intervals. We define a *vector interval* to be a triple of complex intervals. We define a *matrix interval* to be a triple of vector intervals. And so on. We say that a vector interval bounds a vector if the components of the vector interval bound the components of the vector. Likewise for the other structures.

The algebra of the interval structures is identical to the corresponding algebra for the usual structures. At every step of our computation, the actual object is bounded by the corresponding interval version of the object. Thus, if one of our algorithms halts with success, as implemented, the information constitutes a proof that a perfectly accurate computing machine would also halt with success.

12.6 Record of the Calculations

Our code is contained in the directory `res/Computers/Proof`. This directory is contained in the University of Maryland College Park mathnet system.

The calculations from §3.4 are called CALC1 and CALC2, and appear in the Mathematica code in the same order they appear in §3.4. The calculation CALC3 is the calculation for the Year Lemma. The calculation CALC4 establishes the Lemma 9.8. The calculation CALC5 establishes Lemma 9.9. The calculation CALC6 establishes Lemma 11.3. The calculation CALC7 establishes Corollary 11.4. We performed the first 3 calculations on Sep 2, 1999. We performed the remaining 4 calculations on Sep 30, 1999. For all calculations, we used the computer legendre.umd.edu, which is a Sparc Ultra 5.

Our Mathematica code also calculates the five disks used in estimate 1.

We computed these disks on Sept 2, 1999, on the same machine. Here is the result:

1. W_A has center 1.0757057484009542760... and
   radius .3964124835860459412....

2. $W_B^{\pm}$ has center .8425731633320585661... $\pm$ (.13646924571449026840...)i
   and radius .1513081547068024....

3. $W_C^{\pm}$ has center 0.9316949906249123735...$\pm$(0.38927404513542949 27...)i
   and radius .13996370162172745806...

We performed the C Calculations, during the period of Sep 24, 1999 to Sep 28, 1999. We used, in parallel, the following Sparc Ultra 5 workstations

```
legendre.umd.edu
noether.umd.edu
kummer.umd.edu
galois.umd.edu
pascal.umd.edu
sylow.umd.edu
descartes.umd.edu
maclaurin.umd.edu
monge.umd.edu
poisson.umd.edu
simpson.umd.edu
```

These ghosts of famous departed mathematicians all took part in establishing our theorem.

13 Computer Plots

Figure 13.1 shows $\Pi_W(d\Omega_d(\overline{s}))$. The five grey disks are W_{ABC}. The curves in the picture are individual foliating $\boldsymbol{R}$-arcs, which attach to ∂W_2.

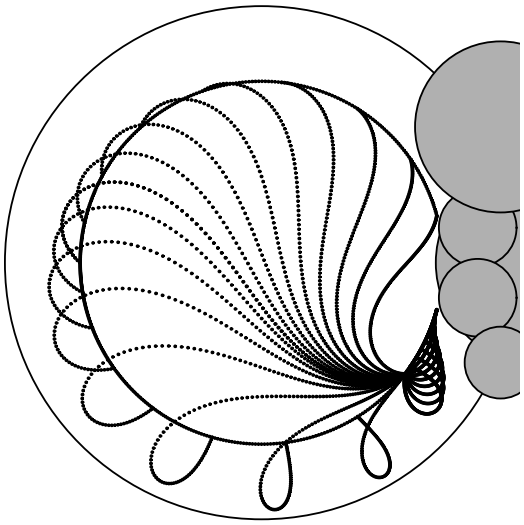

Figure 13.1

Figure 13.2 shows a close up of Figure 13.1, with some additional points plotted.

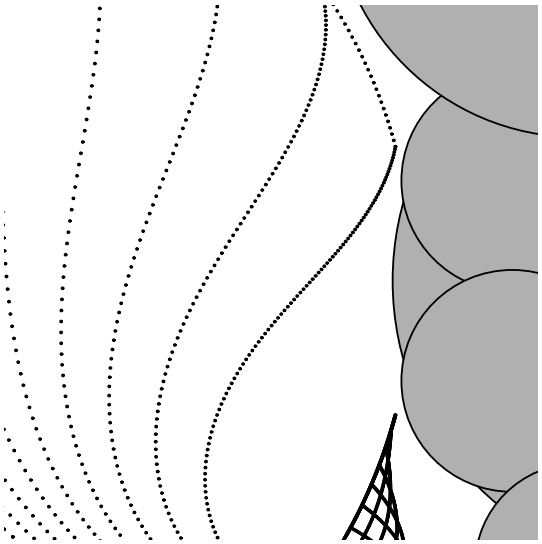

Figure 13.2

Figure 13.3 shows $\Pi_W(d\Omega_h(\overline{s}))$. The five grey disks are W_{ABC}. The curves in the picture are individual foliating $\boldsymbol{R}$-arcs, which attach to ∂W_2.

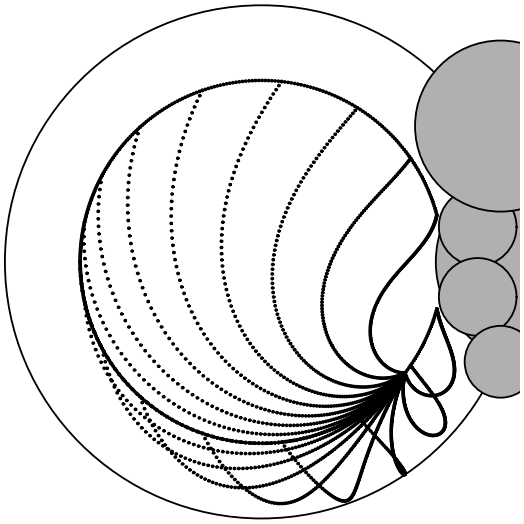

Figure 13.3

Figure 13.4 shows a close up of Figure 13.3, with some additional points plotted.

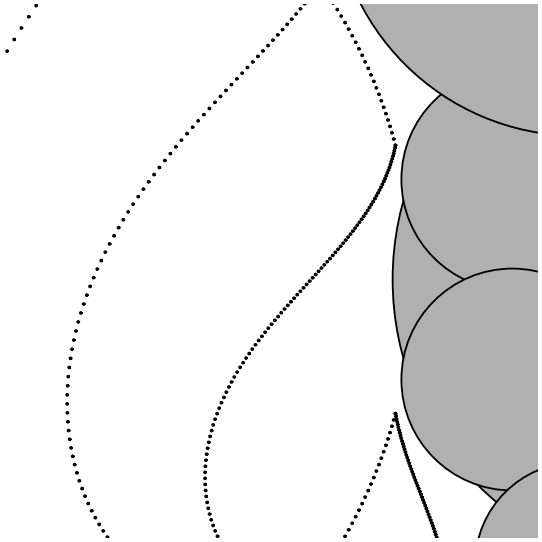

Figure 13.4

Figure 13.5 shows $\Pi_W(d\Omega_h(\overline{s}))$. The five grey disks are W_{ABC}. The curves in the picture are individual foliating $\boldsymbol{R}$-arcs, which attach to ∂W_2.

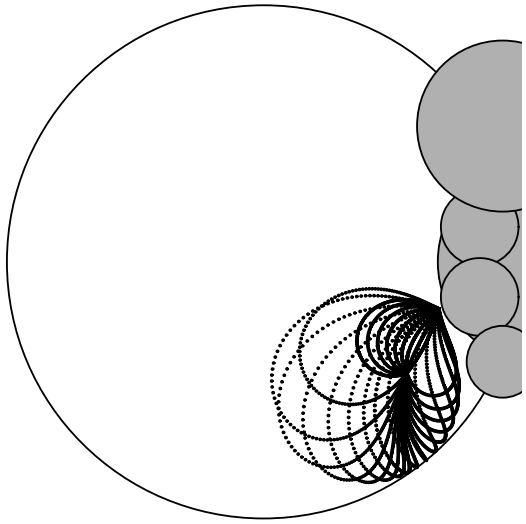

Figure 13.5

Figure 13.6 shows a close up of Figure 13.6, with some additional points plotted.

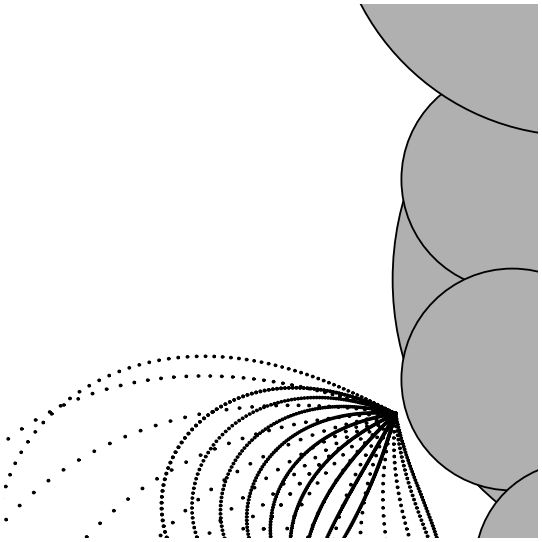

Figure 13.6

Figures 13.7 shows $\Psi_{\overline{s}}(d\Omega_d(\overline{s}))$ and $g_{\overline{s}}(\Psi_{\overline{s}}(d\Omega_d(\overline{s})))$. The cylinder Υ has been identified to $\boldsymbol{R}/2\pi\boldsymbol{Z} \times \boldsymbol{Z}$ via $(u,t) \to (\arg u, t)$. The sine curve is the common boundary of $\Lambda_1(f)$ and $\Lambda_2(f)$, with f as in Equation 50.

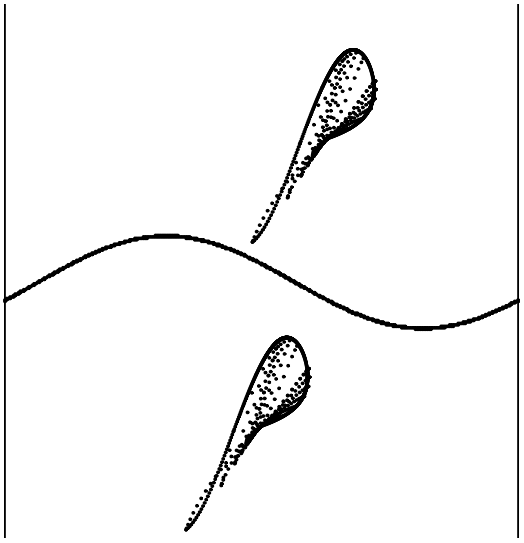

Figure 13.7

Figure 13.8 shows $\Psi_{\overline{s}}(d\Omega_v(\overline{s}))$ and $g_{\overline{s}}(\Psi_{\overline{s}}(d\Omega_v(\overline{s})))$. When h replaces v, the picture looks exactly like Figure 13.8, but rotated 180 degrees about the points of symmetry of $\Lambda(\overline{s})$.

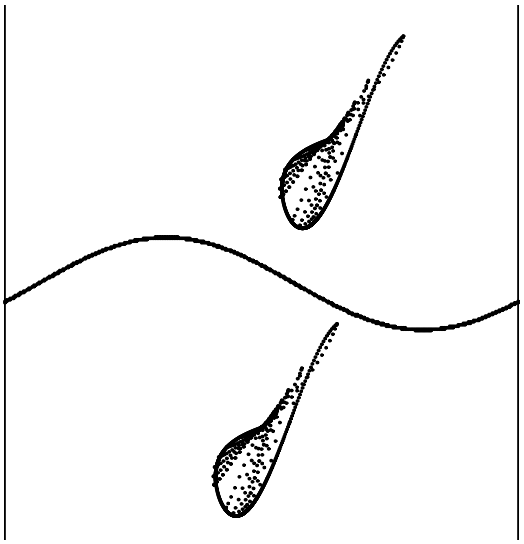

Figure 13.8

In §11 we break Ξ into 5 pieces: $\Xi = \Xi_1 \cup ... \cup \Xi_5$. (Compare Figure 11.1.) Figure 13.11 shows $\Psi_{\overline{s}}(\Xi_2 \cup \Xi_3)$ and $\Psi_{\overline{s}}(g_{\overline{s}}(\Xi_2 \cup \Xi_3)))$.

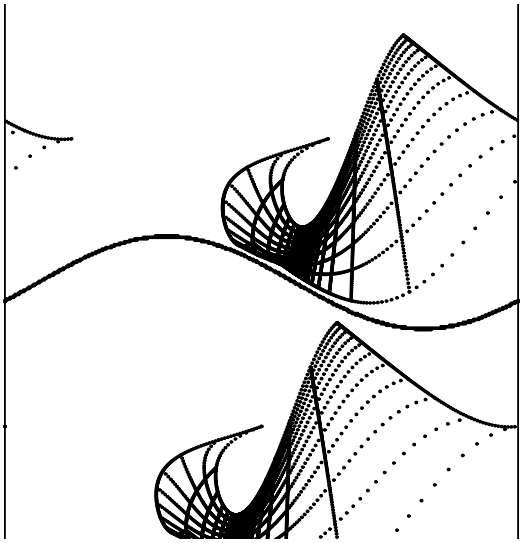

Figure 13.10

Figure 13.11 shows a closeup of Figure 13.10. A somewhat different set of points has been plotted.

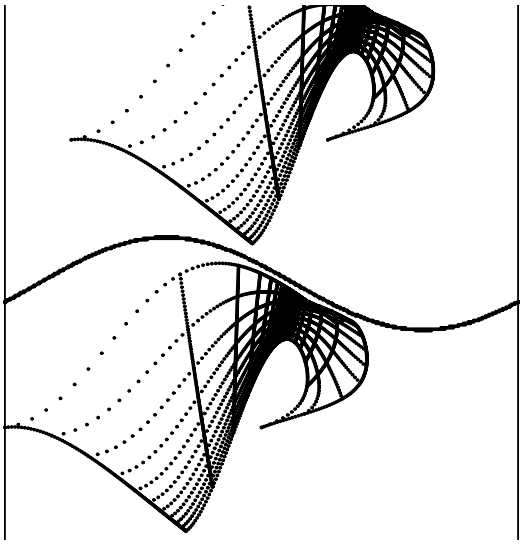

Figure 13.11

Figure 13.12 shows $\Psi_{\overline{s}}(\Xi_1)$ and $\Psi_{\overline{s}}(g_{\overline{s}}(\Xi_1))$.

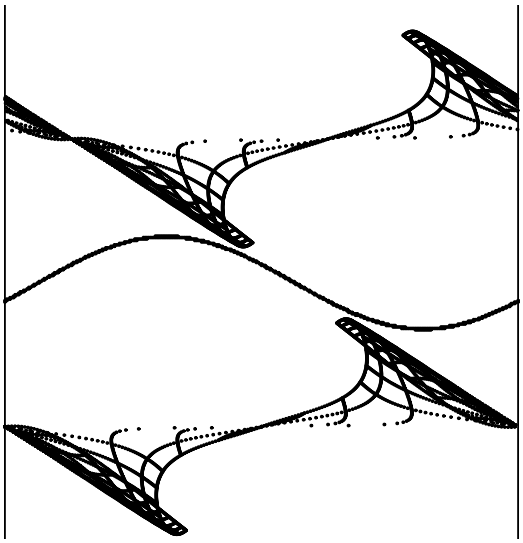

Figure 13.12

We have $r(\Xi_2 \cup \Xi_3) = \Xi_4 \cup \Xi_5$. Thus, the picture for $\Psi_{\overline{s}}(\Xi_4 \cup \Psi_5)$ and $\Psi_{\overline{s}}(g_{\overline{s}}((\Xi_4 \cup \Psi_5))$ is obtained by rotating Figures 13.10 and 13.11 about the point of symmetry on $\Lambda_{\overline{s}}$

14 References

[**E**] D.B.A. Epstein, *Complex Hyperbolic Geometry*, London Mathematical Society Lecture Notes, **111**, 1987

[**FZ**], E. Falbel and V. Zocco, *A Poincare's Fundamental Polyhedron Theorem for Complex Hyperbolic Manifolds*, preprint 1997.

[**G**], W. Goldman, *Complex Hyperbolic Geometry*, Oxford University Press, 1999.

[**GKL**] W. Goldman, M. Kapovich and B. Leeb, *Complex Hyperbolic surfaces homotopy equivalent to a Riemann surface*, Communications in Geometry and Analysis (to appear).

[**GMT**] D. Gabai, R. Meyerhoff, N. Thurston, *Homotopy Hyperbolic Manifolds are Hyperbolic*, Annals of Math (to appear)

[**GP**] W. Goldman and J. Parker, *Complex hyperbolic ideal triangle groups*, J reine agnew. Math **425**, 1992.

[**GuP**], N. Gusevskii and J. Parker, *Complex Hyperbolic Quasifuchsian Surfaces*, preprint 1999.

[**K**] F. Klein, *Neue Beiträge zur Riemannschen Functionentheorie*, Math. Ann. 21 (1883), 141-218.

[**KR**] A. Koranyi and H. M. Reimann, *Quasiconformal Mappings of the Heisenberg Group*, Inventiones, 1985.

[**KeR**] B. Kernighan and D. Ritchie, *The C Programming Language*, Prentice Hall, 1978.

[**I**] *IEEE Standard for Binary Floating-Point Arithmetic*, Institute of Electrical and Electronics Engineers, July 26, 1985

[**M1**], A.M. Macbeath, *Packings, free products and residually finite groups*, Math. Proc. Cambridge Phil. Soc. 59 (1963), 555-558.

[**M2**] B. Maskit, *Construction of Kleinian groups*, Proceedings of Conference on Complex Analysis, Minneapolis 1964, 281-296.

[**Sa**] H. Sandler, *Trace Equivalence in* $SU(2,1)$, Geometriae Dedicata **69** (1998) 317-327

[**S1**] R. Schwartz, *Dented Tori*, 1997
electronic program-document, written in Tcl and C
available upon request to res@math.umd.edu

[**S2**] R. Schwartz, *Degenerating the Complex Hyperbolic Ideal Triangle Groups*, Acta Mathematica (to appear)

[**S3**] R. Schwartz, *Circle Quotients and String Art*, preprint, 2000.

[**S4**] R. Schwartz, *Real Hyperbolic on the Outside, Complex Hyperbolic on the Inside*, preprint, 2000.

[**T**] W. Thurston, *The Geometry and Dymamics of Surface Diffeomophisms*, Bulletin of the A.M.S., Vol. 19., Oct. 1988. Notes, 1978.

[**Tol**], D. Toledo, *Representations of Surface Groups on Complex Hyperbolic Space*, J. Diff. Geo **29** (1989) 125-133.

[**W**] S. Wolfram, *Mathematica: A System for Doing Mathematics by Computer*, 1995.

[**W-G**] J. Wyss-Gallifent, *Complex Hyperbolic Triangle Groups*, Ph.D. Thesis, University of Maryland, 2000.